

**Figure 3** Significantly mutated genes and pathways for 106 ccRCC specimens. The number of somatic mutations in each case (top) and the number of cases that had alterations in significantly mutated genes (bottom right) are shown in a bar plot.

VHL, Elongin B, Elongin C and a catalytic RING subunit (RBX1), which binds ubiquitin-conjugated E2 component, are organized on a cullin scaffold protein (CUL2) to accomplish ubiquitination of VHL-bound HIF proteins (Fig. 2a, left)<sup>22</sup>. Targeted deep sequencing and methylation analysis for the entire cohort identified 8 mutations (3.3%) in *TCEB1*. No mutations were detected in other complex components, including *TCEB2* (encoding Elongin B), *CUL2* and *RBX1*. Together with *VHL* lesions, genetic and epigenetic alterations in the VHL complex accounted for 229 of the 240 ccRCC specimens (95.4%) in which *TCEB1* mutations and *VHL* lesions were completely mutually exclusive ( $P = 2.50 \times 10^{-14}$ , Fisher's exact test), further underscoring the critical role of VHL complex inactivation in the pathogenesis of ccRCC (Fig. 1a). There were no significant differences in the clinicopathological characteristics of cases with mutated *VHL* and those with mutated *TCEB1* (Supplementary Table 6).

Whereas *VHL* mutations and methylation were closely associated with LOH at 3p, *TCEB1* mutations were always accompanied by loss of chromosome 8 ( $P = 3.03 \times 10^{-9}$ , Fisher's exact test), leading to complete loss of wild-type *TCEB1* alleles (on 8q21) (Fig. 1a). However, in contrast to *VHL* mutations of which nonsense or frameshift alterations frequently result in complete loss of protein function, *TCEB1* mutations exclusively involved two conserved amino acids, Tyr79 ( $n = 7$ ) and Ala100 ( $n = 1$ ), with the former being a mutational hotspot (Fig. 2b and Supplementary Fig. 10). Notably, these two amino acids are positioned close together within the binding interface for the VHL protein (Fig. 2c): Tyr79 mediates a hydrogen bond with Pro154 of VHL via a water molecule (Fig. 2d), and Ala100 participates in hydrophobic interactions with Val165 and Val166 of VHL (Fig. 2e)<sup>23,24</sup>. Thus, mutations that affect these two amino acids (p.Tyr79Cys, p.Tyr79Ser and p.Ala100Pro) are predicted to abolish the interaction between Elongin C and VHL and to result in compromised ubiquitination and subsequent accumulation of HIF (Fig. 2f–h).

Indeed, when expressed in HEK 293T cells, wild-type Elongin C effectively coprecipitated with VHL and CUL2, whereas the interaction with VHL and CUL2 was markedly reduced with mutant Elongin C (Tyr79Cys and Ala100Pro; Fig. 2i and Supplementary Fig. 11a). We also examined the effects of mutant Elongin C on HIF-1 $\alpha$  accumulation by exogenously expressing various Elongin C proteins in HeLa cells. As expected, HIF-1 $\alpha$  accumulation was not observed after simply expressing these putative loss-of-function Elongin C mutants or the wild-type protein (Fig. 2j, left). However, when endogenous wild-type Elongin C expression was suppressed by small interfering RNA (siRNA) specific for the endogenous *TCEB1* transcripts (Online Methods and Supplementary Table 7a), both mock-transduced cells and mutant *TCEB1*-transduced cells but not wild-type *TCEB1*-transduced cells showed recognizable HIF-1 $\alpha$  accumulation (Fig. 2j, right). These results suggest that the two *TCEB1* mutants (encoding Tyr79Cys and Ala100Pro) actually represent loss-of-function alleles with regard to VHL complex function and that biallelic inactivation is required for HIF-1 $\alpha$  accumulation, explaining why *TCEB1* mutations were always accompanied by a deletion of the intact *TCEB1* allele on chromosome 8.

Finally, to confirm the oncogenic role of these *TCEB1* mutations in primary ccRCC, we investigated HIF-1 $\alpha$  and HIF-2 $\alpha$  expression in primary surgical ccRCC specimens with *TCEB1* mutations by immunohistochemistry. As with *VHL*-mutated tumors, all five tumors with *TCEB1* mutation exhibited increased HIF-1 $\alpha$  expression in immunohistochemistry compared to normal kidney samples or tumors that lacked *TCEB1* and *VHL* mutations (Fig. 2k, Supplementary Fig. 12 and Supplementary Table 8).

#### Other recurrent mutations

Other newly identified recurrent mutational targets included *TET2*, *KEAP1* and *MTOR* (Fig. 3). *TET2* encodes an  $\alpha$ -ketoglutarate-dependent oxygenase frequently inactivated in myeloid malignancies by gene

mutation<sup>25,26</sup>. TET2 catalyzes the conversion of 5-methylcytosine to 5-hydroxymethylcytosine, which is now believed to be a critical step in DNA demethylation. A recent study indicated that TET2 also mediates histone O-GlcNAcylation during gene transcription<sup>27</sup>. No TET2 mutations have been reported in non-hematopoietic tumors, except for rare mutations in colorectal cancers (5/214 examined; 2.3%)<sup>28</sup>. TET2 was mutated in 6 of 106 ccRCC cases (5.7%). Except for one frameshift mutation, five were missense mutations, of which four affected the cysteine-rich or catalytic domain (Supplementary Fig. 13a). In copy number analysis using SNP arrays (Fig. 4), TET2 was also located within the significantly deleted regions at 4q24 ( $n = 11$ ; 10.4%) (Fig. 4f). In combination, TET2 mutations and deletions accounted for 17 ccRCC cases (16.0%), with no case having biallelic inactivation that indicated a haploinsufficiency effect of TET2 on the pathogenesis of ccRCC. KEAP1 is a key component of another cullin-RING ubiquitin ligase complex that is involved in oxidative stress responses by regulating the ubiquitination of the KEAP1-bound NRF2 transcription factor (also known as NEF2L2) (Fig. 2a, right)<sup>29</sup>. Frequent KEAP1 and NRF2 mutations that abrogate their physical interaction were originally reported in squamous cell carcinoma of the lung and in other solid cancers<sup>30–32</sup>,

with KEAP1-mediated NRF2 degradation compromised, resulting in deregulated transcriptional activity of the abnormally accumulated NRF2. Of note, compromised KEAP1-mediated NRF2 degradation is also caused by abnormally accumulated fumarate in congenital fumarate hydratase deficiency<sup>33,34</sup>, which predisposes to type 2 papillary renal cell carcinoma (pRCC2), and also by somatic mutations in NRF2 and CUL3 in sporadic cases with pRCC2 (ref. 35). The current study confirmed that mutually exclusive mutations in KEAP1 ( $n = 5$ ), NRF2 ( $n = 1$ ) and CUL3 ( $n = 1$ ) are also found in the clear-cell subtypes of RCC (6.6%) (Supplementary Fig. 14), together with deletions in the CUL3 locus at 2q36 ( $n = 11$ ; 10.4%) (Fig. 4d), with no case having biallelic inactivation in this pathway. MTOR was also a newly identified recurrent mutational target and was mutated in 6 of 106 ccRCC cases (5.7%), although a single case with an activating MTOR mutation was previously reported<sup>17</sup>. Together with mutations in PTEN ( $n = 2$ ), PIK3CA ( $n = 5$ ), PIK3CG ( $n = 2$ ), RPS6KA2 ( $n = 3$ ), TSC1 and TSC2 (ref. 36) ( $n = 2$ ), and other genes, a total of 28 cases (26%) had mutations that involved phosphoinositide 3-kinase (PI3K)-AKT-mTOR signaling. Except for 3 known tumor suppressor genes—PTEN, TSC1 and TSC2—27 mutations were found in 13 genes that are thought to functionally act as oncogenes. In fact, none of the 27 mutations were nonsense, frameshift or splice-site changes, which was highly unexpected from the observed overall frequencies of these types of mutations in ccRCC ( $P = 0.00946$ , Fisher's exact test), suggesting that these mutations largely act as oncogenes. These mutations were mutually exclusive, except for in two cases that had both PTEN and AKT2 mutations. FGFR4 was within the significantly amplified region at 5q35 ( $n = 69$ ), and, in total, 81 cases (76%) had genetic alterations in this pathway (Fig. 5a). These findings provide additional rationale for the effectiveness of mTOR inhibitors in ccRCC.

#### Copy number lesions and significantly affected pathways

We also performed SNP array-based copy number analysis for the 240 ccRCC specimens to identify candidate target genes involved in pathogenesis. Most copy number lesions involved large chromosomal segments, as found in LOH at 3p (94%), gain of 5q (65%), gain of 7q (41%), loss of 8p with or without loss of 8q (20%), LOH at 9p (15%), LOH at 14q (27%) and LOH at 18q (11%) (Supplementary Fig. 15a). Even though there was a close correlation between monosomy 8 and TCEB1 mutation, total or partial loss of chromosome 8 was also found in cases with wild-type TCEB1, in which common loss of 8p seemed to be relevant to ccRCC pathogenesis. Hyperploid tumors (defined by ploidy of  $>2.5$ ) accounted for 17.5% ( $n = 42$ ) of the cases and had a significantly higher rate of metastasis ( $P = 2.98 \times 10^{-5}$ , Cox proportional hazards model) and poor prognosis ( $P = 3.93 \times 10^{-2}$ , Cox proportional hazards model). In hyperploid tumors, copy numbers in LOH involving 3p, 9p and 14q were largely neutral, suggesting that these tumors had evolved from diploid tumors with typical deletions of the relevant chromosome segments (Supplementary Fig. 15b,c). Supporting this notion was the fact that mutations in the 3p target genes in cases with UPD at 3p showed higher allele frequencies than those for mutations within  $2N$  regions (Supplementary Fig. 16). Using GISTIC 2.0 analysis, significant focal gains and deletions ( $q < 0.25$ ) were found at 20 loci (5 gains and 15 losses) that involved known tumor suppressors and oncogenes, including ARID1A (1p36.11), CUL3 (2q36.2), FHIT (3p14.2), TET2 (4q24), ARID1B (6q25.2), CDKN2A and CDKN2B (9p21.3), PBX1 (1q23.3), FGFR4 (5q35.2) and MYC (8q24) (Fig. 4).

Significantly affected pathways in ccRCC were further investigated by searching for statistically overrepresented gene families that were somatically mutated and expressed and/or showed copy number abnormalities (Online Methods). In addition to PI3K-AKT-mTOR signaling, significantly affected pathways (false discovery rate

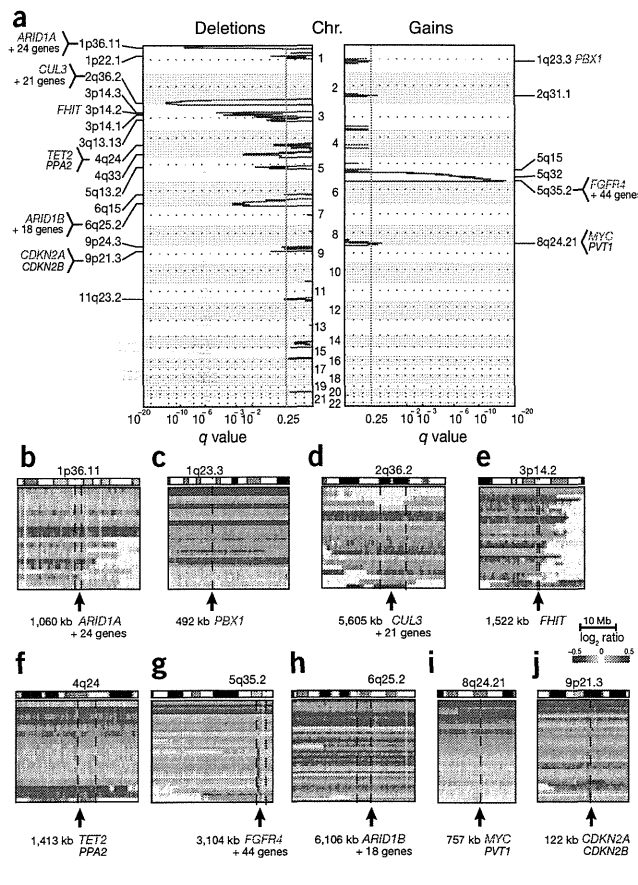


**Figure 4** Significant copy number alterations in 240 ccRCC specimens. (a) Regions showing statistically significant increase or decrease in genomic copy number were detected using the GISTIC algorithm based on SNP array analysis. For each  $q$ -value peak, putative gene targets are listed. A dashed line represents the centromere of each chromosome. Red and blue lines indicate  $q$  value for gains and deletions, respectively. (b–j) Log-ratio copy number heatmaps are shown for gene targets at 1p36.11 (b), 1q23.3 (c), 2q36.2 (d), 3p14.2 (e), 4q24 (f), 5q35.2 (g), 6q25.2 (h), 8q24.21 (i) and 9p21.3 (j).

(FDR) < 0.01) included p53 signaling and cell cycle checkpoints, mRNA processing and the SWI/SNF complex (Supplementary Fig. 13b and Supplementary Table 9). *TP53* was mutated in only 3 cases (2.8%), but, considering these cases together with those with mutations in *ATM* ( $n = 2$ ), *CHEK2* ( $n = 1$ ), *MDM2* ( $n = 1$ ) and *E2F3* ( $n = 1$ ), copy number deletions in *CDKN2A* at 9p21 ( $n = 17$ ; including 4 homodeletions) and gains in *MYC* at 8q24 ( $n = 24$ ), a total of 42 cases (40%) had genetic alterations involved in p53 signaling and/or cell cycle checkpoints (Fig. 5b). The pathways involved in mRNA processing were not previously implicated in ccRCC. Frequent mutations in splicing machinery were reported in myelodysplastic syndromes (MDS) and in other hematopoietic neoplasms, with mutations affecting spliceosome components involved in recognizing the 3' splice site<sup>37</sup>. In contrast, in ccRCC, mutated genes that were involved in mRNA processing were related to later steps in splicing, including the release of introns, 3' end processing and mRNA export to the cytoplasm (Supplementary Fig. 13c).

*PBRM1* was the second most commonly mutated gene in ccRCC and encodes a component of the SWI/SNF complex that regulates chromatin structure through ATP-dependent nucleosome remodeling. Other components of the SWI/SNF complex, including *ARID1A* and *ARID1B*, were within significantly deleted regions at 1p36 and 6q25, respectively. Taking into consideration these cases and those with mutations in *ARID1A* ( $n = 2$ ), *SMARCA2* ( $n = 2$ ), *SMARCA4* ( $n = 2$ ), *SMARCB1* ( $n = 2$ ) and other genes, a total of 61 cases (58%) had mutations and/or deletions in 11 different components of the SWI/SNF complex (Fig. 5c). These changes were not mutually exclusive, and 5 cases had  $\geq 2$  mutations. Multiple components of the SWI/SNF complex might be mutated in single cases in various types of cancer<sup>38</sup>. Notably, these five ccRCC cases had significantly worse prognosis compared to individuals with less than two mutations in the SWI/SNF complex (HR = 5.40, 95% CI = 1.56–14.5;  $P = 0.0113$ ; Cox proportional hazards model), indicating that multiple mutations in the SWI/SNF complex could lead to aggressive phenotype in ccRCC.

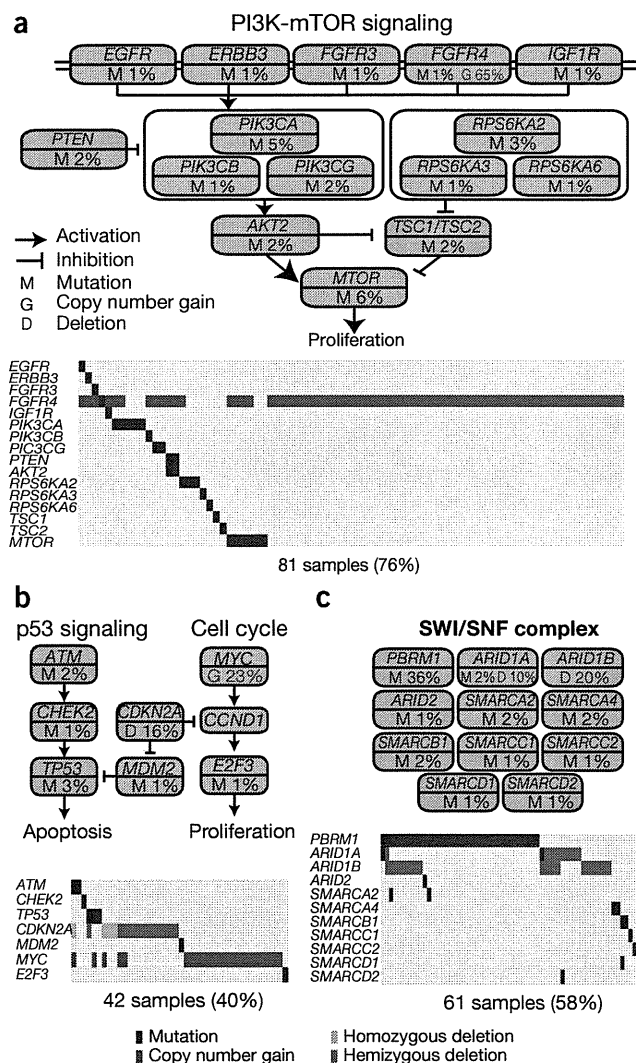


**Figure 5** Significantly mutated pathways for 106 ccRCC specimens. (a–c) PI3K-mTOR signaling (a), p53 signaling (b) and the SWI/SNF complex (c) are commonly altered in ccRCC. Alterations are defined as somatic mutations and DNA copy number changes identified by GISTIC 2.0 analysis. Genes considered to be oncogenes or tumor suppressor genes are colored pink and blue, respectively.

### Integrated molecular analysis of ccRCC

RNA sequencing was also performed in 100 ccRCC cases (Supplementary Table 10). In total, 44 fusion transcripts were identified in 25 specimens (Supplementary Table 11), of which about one-third ( $n = 14$ ) were in frame. The lack of recurrent lesions largely obscured the significance of these fusions, except for *SETD2-QRICH1* and *NONO-TFE3* fusions. *TFE3* on Xp11 participates in promiscuous gene fusions with several partners, including *NONO*<sup>39</sup>. *TFE3*-containing fusions have been implicated in RCCs that are histologically distinct from typical ccRCCs (RCCs with Xp11 translocation)<sup>39,40</sup>. The current case with a *NONO-TFE3* fusion was positive for *TFE3* expression in immunohistochemistry but showed histology otherwise indistinguishable from that typical for ccRCC cases<sup>41</sup> (Supplementary Fig. 17).

As previously reported, gene expression profiling of 101 ccRCC cases identified 2 major clusters—ccA and ccB—which were characterized by upregulated angiogenic factors and enhanced expression of genes involved in cell cycle progression, respectively (Supplementary Fig. 18a–c)<sup>42</sup>. In accordance with recent reports<sup>10,20</sup>, Gene Set Enrichment Analysis (GSEA) showed discrete expression profiles in *BAP1*- and *PBRM1*-mutated tumors. *PBRM1*-mutated tumors were enriched for upregulated expression of the gene set with a hypoxia signature, whereas *BAP1*-mutated cases were associated with downregulated expression of target genes of polycomb repressive complex 2 (PRC2) (Supplementary Fig. 19).

DNA methylation profiling based on hierarchical clustering identified 3 distinct clusters that were characterized by different DNA methylation levels, including clusters with high, intermediate and low mean methylation levels, as determined using a total of 1,288 differentially methylated genes (Fig. 6a, Online Methods and Supplementary Fig. 20). Functional annotation analysis using The Database for Annotation, Visualization and Integrated Discovery (DAVID)<sup>43</sup> showed over-representation of homeobox genes in the 1,228 differentially methylated genes (Supplementary Table 12), and GSEA of the differentially methylated genes in the high and low-intermediate subgroups showed a marked enrichment in the cluster with high methylation of the gene set regulated by PRC2 and of the genes undergoing methylation at histone H3 lysine 27 (H3K27) (Fig. 6b). The cluster with high methylation was also characterized by a higher *BAP1* mutation rate ( $P = 5.22 \times 10^{-3}$ ) and lower *BAP1* ( $P = 2.11 \times 10^{-2}$ ) and higher *EZH2* ( $P = 1.57 \times 10^{-5}$ ) expression levels (Fig. 6c,d). Notably, *BAP1* mutation ( $P = 4.86 \times 10^{-3}$ ), decreased *BAP1* expression ( $P = 7.46 \times 10^{-3}$ ) and increased *EZH2* expression ( $P = 8.10 \times 10^{-3}$ ) were shown to be significantly associated with increased methylation of PRC2 target genes (Supplementary Fig. 21). These

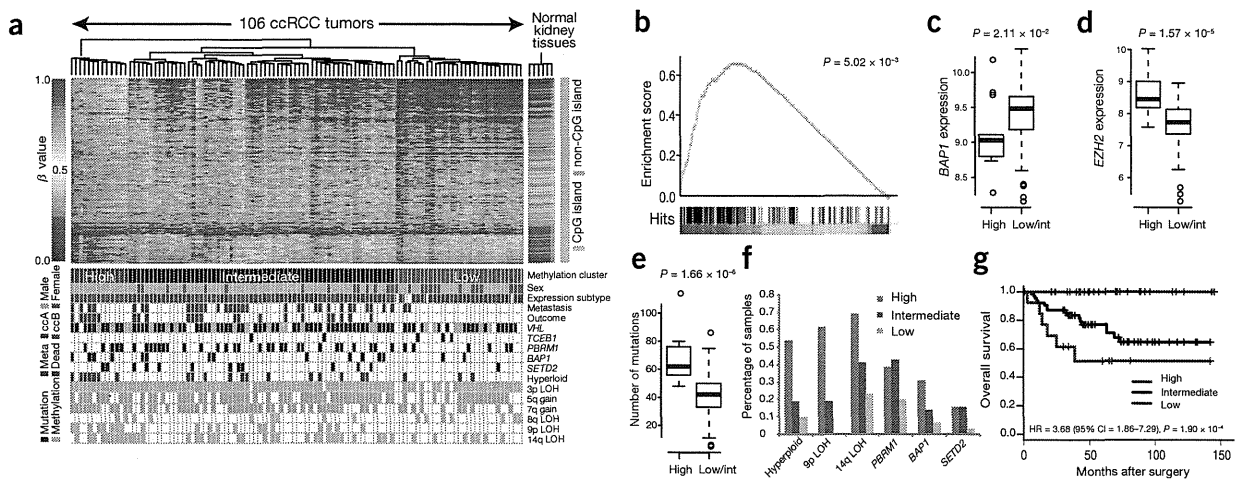


**Figure 6** Correlations between DNA methylation and other genetic lesions. **(a)** Integrated view of DNA methylation clustering combined with mutation status of common driver genes, gene expression profiles and genome copy numbers.  $\beta$  values are for DNA methylation. Probes corresponding to CpG islands and non-CpG islands are shown on the right. Clinical outcomes and the presence-absence of metastasis are also shown. Meta, cases with distant metastasis. **(b)** GSEA showing significant enrichment of PRC2-regulated genes in differentially methylated genes in the subgroup with high DNA methylation. Hits displayed below the graph show where the members of the gene set appear in the ranked list of genes. **(c–g)** Integrated genetic and epigenetic analyses showed close correlation between DNA methylation status and *BAP1* expression **(c)**, *EZH2* expression **(d)**, total number of somatic mutations **(e)**, hyperploidy, LOH at 9p, LOH at 14q and *PBRM1*, *BAP1* and *SETD2* mutations **(f)** and clinical outcome **(g)**. *P* values were calculated using the *t* test in **c–e**, the Cochran-Armitage trend test in **f** and the log-rank test in **g**. Box plots show median, 25% and 75% quartile ranges.

findings strongly indicate that the cluster with high methylation was closely related to deregulated PRC2 activity.

Other prominent features of the cluster with high methylation included a higher number of somatic mutations ( $P = 1.66 \times 10^{-6}$ ), more hyperplid cases ( $P = 1.57 \times 10^{-3}$ ), cases with LOH at 14q ( $P = 2.0 \times 10^{-4}$ ) and 9p ( $P = 1.57 \times 10^{-3}$ ), enrichment of the ccB gene expression profile ( $P = 2.46 \times 10^{-10}$ ) (Fig. 6a,e,f) and strong association with higher probability of metastasis (HR = 1.96, 95% CI = 1.17–3.30;  $P = 1.11 \times 10^{-2}$ ) and poor overall survival (HR = 3.68, 95% CI = 1.86–7.29;  $P = 1.90 \times 10^{-4}$ ) (Fig. 6g), which combined with the deregulated PRC2 profile, indicate that deregulation of polycomb-mediated gene silencing may contribute to aggressive tumor phenotype and poor clinical outcome.

## DISCUSSION

Our comprehensive molecular study involving 106 ccRCC cases provided new insights into ccRCC genetics and biology and identified potential therapeutic targets. Similar to what has been observed in other cancers, the development of ccRCC seems to be shaped by the acquisition of a number of somatic gene mutations and chromosomal lesions that predominantly affect a handful of genes (*VHL*, *PBRM1*, *SETD2* and *BAP1*) and chromosome regions (3p, 5q, 9p and 14q), with many less frequent mutations additionally occurring in key targets. Pathway analysis of gene mutations disclosed several functional gene pathways, including PI3K-AKT-mTOR signaling, the KEAP1-NRF2 apparatus and mRNA processing, that were commonly affected by multiple, less frequent mutations.

A cardinal feature of ccRCC is a very high frequency of *VHL* inactivation caused by gene deletion, mutation and/or silencing via promoter methylation, leading to HIF accumulation. From this perspective, the discovery of *TCEB1* mutations and the obligatory loss of chromosome 8 in 36–42% of ccRCC cases with intact *VHL* was among the most notable findings of this study, demonstrating a new mechanism for inactivation of the VHL complex during ccRCC pathogenesis. These changes not only abolished the recruitment of VHL to the CUL2-RING

ubiquitin ligase complex (CRL2), resulting in HIF accumulation, but could also compromise the recruitment of Elongin A, which is an essential component of the RNA polymerase II Elongin complex<sup>21</sup>, and of other BC-box proteins, such as SOCS3, FEM1B and LRR1, to the CRL2 complex via Elongin C (Supplementary Fig. 11b–e). Loss of chromosome 8 was obligatory and resulted in the total loss of wild-type *TCEB1* alleles. Nevertheless, no nonsense or truncating *TCEB1* mutations were observed, suggesting that mutated Elongin C could still retain its interactions with unknown molecules, which would be critical for tumor cell viability.

By integrating multiple layers of different comprehensive analyses, we unmasked unique correlations between somatic mutations, DNA methylation, gene expression and copy number alterations, which were also closely linked to the clinical behaviors of tumors. In particular, correlation of the cluster with hypermethylation with hyperplid status, LOH at 9p and poor prognosis was conspicuous and was in stark contrast to the correlation of the cluster with low methylation with less frequent hyperplid or LOH at 9p and an excellent prognosis. Clinically, the discovery of the cluster of cases with hypermethylation was a notable finding, and special attention should be paid to these cases in their management and in early detection or prevention of recurrent and/or metastatic disease. Except for frequent hyperplid and a higher *BAP1* mutation rate, the genetic basis of this cluster of cases with hypermethylation remains unclear and will require further investigation to clarify its pathophysiology.

**URLs.** dbSNP, <http://www.ncbi.nlm.nih.gov/projects/SNP/>; 1000 Genomes Project, <http://www.1000genomes.org/>; RepeatMasker, <http://www.repeatmasker.org/>; Genomon-fusion (in Japanese), <http://genomon.hgc.jp/rna/>; CNAG/AsCNAR, <http://www.genome.umin.jp/>; GISTIC 2.0, [http://www.broadinstitute.org/cgi-bin/cancer/publications/pub\\_paper.cgi?mode=view&paper\\_id=216&p=t](http://www.broadinstitute.org/cgi-bin/cancer/publications/pub_paper.cgi?mode=view&paper_id=216&p=t); Gene Set Enrichment Analysis (GSEA), <http://www.broadinstitute.org/gsea/>; MSigDB,

<http://www.broadinstitute.org/gsea/msigdb/index.jsp>; the European Genome-phenome Archive, <https://www.ebi.ac.uk/ega/>.

## METHODS

Methods and any associated references are available in the online version of the paper.

**Accession code.** Sequencing and genotype data have been deposited in the European Genome-phenome Archive (EGA) under accession EGAS00001000509.

*Note: Any Supplementary Information and Source Data are available in the online version of the paper.*

## ACKNOWLEDGMENTS

We thank Y. Mori, M. Nakamura, N. Mizota and S. Ichimura for their technical assistance. We also thank M. Nangaku and N. Takeda for fruitful discussion and comments. We thank T. Kitamura (University of Tokyo) for providing pMXs-puro, M. Onodera (National Center for Child Health and Development, Japan) for providing pGCDNsamIRESEGF and R.C. Mulligan (Boston Children's Hospital) for providing 293gp cells. This work was supported by KAKENHI (22134006), the Industrial Technology Research Grant Program from the New Energy and Industrial Technology Development Organization (NEDO) (08C46598a) and the Japan Society for the Promotion of Science through the Funding Program for World-Leading Innovative R&D on Science and Technology, initiated by the Council for Science and Technology Policy.

## AUTHOR CONTRIBUTIONS

Y. Sato, S. Maekawa, Y.N., H.S., Y. Suzuki, S.S., K.Y. and A.K. performed DNA sequencing. Y. Shiraishi, Y.O., K.C., H.T., A.F., T.T. and S. Miyano performed bioinformatics analyses of the sequencing data. T.Y., M.S. and T.K. performed the functional analyses of Elongin C mutants. Y. Sato, A.S.-O., A.N. and M.S. performed SNP array and expression array analyses. T.S., G.N. and H.A. performed methylation analysis. H.K. and Y.H. provided specimens and were also involved in planning the project. T.M., D.M. and M.F. confirmed histological diagnosis and performed immunostaining for HIF proteins. Y. Sato, T.Y., Y.O., A.S.-O. and S.O. generated figures and tables and wrote the manuscript. S.O. led the entire project. All authors participated in the discussion and interpretation of data and results.

## COMPETING FINANCIAL INTERESTS

The authors declare no competing financial interests.

Reprints and permissions information is available online at <http://www.nature.com/reprints/index.html>.

- Ferlay, J. *et al.* Estimates of worldwide burden of cancer in 2008: GLOBOCAN 2008. *Int. J. Cancer* **127**, 2893–2917 (2010).
- Rini, B.I., Campbell, S.C. & Escudier, B. Renal cell carcinoma. *Lancet* **373**, 1119–1132 (2009).
- Ljungberg, B. *et al.* EAU guidelines on renal cell carcinoma: the 2010 update. *Eur. Urol.* **58**, 398–406 (2010).
- Gnarra, J.R. *et al.* Mutations of the *VHL* tumour suppressor gene in renal carcinoma. *Nat. Genet.* **7**, 85–90 (1994).
- Gallou, C. *et al.* Mutations of the *VHL* gene in sporadic renal cell carcinoma: definition of a risk factor for VHL patients to develop an RCC. *Hum. Mutat.* **13**, 464–475 (1999).
- Schraml, P. *et al.* *VHL* mutations and their correlation with tumour cell proliferation, microvessel density, and patient prognosis in clear cell renal cell carcinoma. *J. Pathol.* **196**, 186–193 (2002).
- Herman, J.G. *et al.* Silencing of the *VHL* tumor-suppressor gene by DNA methylation in renal carcinoma. *Proc. Natl. Acad. Sci. USA* **91**, 9700–9704 (1994).
- Varela, I. *et al.* Exome sequencing identifies frequent mutation of the SWI/SNF complex gene *PBRM1* in renal carcinoma. *Nature* **469**, 539–542 (2011).
- Dalglish, G.L. *et al.* Systematic sequencing of renal carcinoma reveals inactivation of histone modifying genes. *Nature* **463**, 360–363 (2010).
- Peña-Llopis, S. *et al.* *BAP1* loss defines a new class of renal cell carcinoma. *Nat. Genet.* **44**, 751–759 (2012).
- Guo, G. *et al.* Frequent mutations of genes encoding ubiquitin-mediated proteolysis pathway components in clear cell renal cell carcinoma. *Nat. Genet.* **44**, 17–19 (2012).
- Greenman, C. *et al.* Patterns of somatic mutation in human cancer genomes. *Nature* **446**, 153–158 (2007).
- Guichard, C. *et al.* Integrated analysis of somatic mutations and focal copy-number changes identifies key genes and pathways in hepatocellular carcinoma. *Nat. Genet.* **44**, 694–698 (2012).
- Huang, J. *et al.* Exome sequencing of hepatitis B virus-associated hepatocellular carcinoma. *Nat. Genet.* **44**, 1117–1121 (2012).
- Sung, W.K. *et al.* Genome-wide survey of recurrent HBV integration in hepatocellular carcinoma. *Nat. Genet.* **44**, 765–769 (2012).
- Fujimoto, A. *et al.* Whole-genome sequencing of liver cancers identifies etiological influences on mutation patterns and recurrent mutations in chromatin regulators. *Nat. Genet.* **44**, 760–764 (2012).
- Gerlinger, M. *et al.* Intratumor heterogeneity and branched evolution revealed by multiregion sequencing. *N. Engl. J. Med.* **366**, 883–892 (2012).
- Hakimi, A.A. *et al.* Adverse outcomes in clear cell renal cell carcinoma with mutations of 3p21 epigenetic regulators *BAP1* and *SETD2*: a report by MSKCC and the KIRC TCGA Research Network. *Clin. Cancer Res.* **19**, 3259–3267 (2013).
- Hakimi, A.A. *et al.* Clinical and pathologic impact of select chromatin-modulating tumor suppressors in clear cell renal cell carcinoma. *Eur. Urol.* **63**, 843–854 (2013).
- Kapur, P. *et al.* Effects on survival of *BAP1* and *PBRM1* mutations in sporadic clear-cell renal-cell carcinoma: a retrospective analysis with independent validation. *Lancet Oncol.* **14**, 159–167 (2013).
- Aso, T., Lane, W.S., Conaway, J.W. & Conaway, R.C. Elongin (SIII): a multisubunit regulator of elongation by RNA polymerase II. *Science* **269**, 1439–1443 (1995).
- Kamura, T. *et al.* Activation of HIF1a ubiquitination by a reconstituted von Hippel-Lindau (VHL) tumor suppressor complex. *Proc. Natl. Acad. Sci. USA* **97**, 10430–10435 (2000).
- Stebbins, C.E., Kaelin, W.G. Jr. & Pavletich, N.P. Structure of the VHL-ElonginC-ElonginB complex: implications for VHL tumor suppressor function. *Science* **284**, 455–461 (1999).
- Takagi, Y., Pause, A., Conaway, R.C. & Conaway, J.W. Identification of elongin C sequences required for interaction with the von Hippel-Lindau tumor suppressor protein. *J. Biol. Chem.* **272**, 27444–27449 (1997).
- Delhommeau, F. *et al.* Mutation in *TET2* in myeloid cancers. *N. Engl. J. Med.* **360**, 2289–2301 (2009).
- Langemeijer, S.M. *et al.* Acquired mutations in *TET2* are common in myelodysplastic syndromes. *Nat. Genet.* **41**, 838–842 (2009).
- Chen, Q., Chen, Y., Bian, C., Fujiki, R. & Yu, X. TET2 promotes histone O-GlcNAcylation during gene transcription. *Nature* **493**, 561–564 (2013).
- The Cancer Genome Atlas Network. Comprehensive molecular characterization of human colon and rectal cancer. *Nature* **487**, 330–337 (2012).
- Zimmerman, E.S., Schulman, B.A. & Zheng, N. Structural assembly of cullin-RING ubiquitin ligase complexes. *Curr. Opin. Struct. Biol.* **20**, 714–721 (2010).
- Padmanabhan, B. *et al.* Structural basis for defects of Keap1 activity provoked by its point mutations in lung cancer. *Mol. Cell* **21**, 689–700 (2006).
- Shibata, T. *et al.* Cancer related mutations in *NRF2* impair its recognition by Keap1-Cul3 E3 ligase and promote malignancy. *Proc. Natl. Acad. Sci. USA* **105**, 13568–13573 (2008).
- Kim, Y.R. *et al.* Oncogenic *NRF2* mutations in squamous cell carcinomas of oesophagus and skin. *J. Pathol.* **220**, 446–451 (2010).
- Adam, J. *et al.* Renal cyst formation in Fh1-deficient mice is independent of the Hif/Phd pathway: roles for fumarate in KEAP1 succination and Nrf2 signaling. *Cancer Cell* **20**, 524–537 (2011).
- Kinch, L., Grishin, N.V. & Brugarolas, J. Succination of Keap1 and activation of Nrf2-dependent antioxidant pathways in FH-deficient papillary renal cell carcinoma type 2. *Cancer Cell* **20**, 418–420 (2011).
- Ooi, A. *et al.* *CUL3* and *NRF2* mutations confer an NRF2 activation phenotype in a sporadic form of papillary renal cell carcinoma. *Cancer Res.* **73**, 2044–2051 (2013).
- Kucejova, B. *et al.* Interplay between pVHL and mTORC1 pathways in clear-cell renal cell carcinoma. *Mol. Cancer Res.* **9**, 1255–1265 (2011).
- Yoshida, K. *et al.* Frequent pathway mutations of splicing machinery in myelodysplasia. *Nature* **478**, 64–69 (2011).
- Kadoch, C. *et al.* Proteomic and bioinformatic analysis of mammalian SWI/SNF complexes identifies extensive roles in human malignancy. *Nat. Genet.* **45**, 592–601 (2013).
- Clark, J. *et al.* Fusion of splicing factor genes *PSF* and *NonO* (*p54<sup>nonO</sup>*) to the *TFE3* gene in papillary renal cell carcinoma. *Oncogene* **15**, 2233–2239 (1997).
- Ross, H. & Argani, P. Xp11 translocation renal cell carcinoma. *Pathology* **42**, 369–373 (2010).
- Kuroda, N. *et al.* Review of renal carcinoma associated with Xp11.2 translocations/*TFE3* gene fusions with focus on pathobiological aspect. *Histol. Histopathol.* **27**, 133–140 (2012).
- Brannon, A.R. *et al.* Molecular stratification of clear cell renal cell carcinoma by consensus clustering reveals distinct subtypes and survival patterns. *Genes Cancer* **1**, 152–163 (2010).
- Huang, W., Sherman, B.T. & Lempicki, R.A. Systematic and integrative analysis of large gene lists using DAVID bioinformatics resources. *Nat. Protoc.* **4**, 44–57 (2009).





## ONLINE METHODS

**Subjects and materials.** Paired tumor-normal DNA was isolated from 240 ccRCC specimens and subjected to comprehensive molecular analyses after written informed consent was obtained. Matched normal specimens for germline controls were obtained from adjacent normal kidney tissue or from peripheral blood specimens (**Supplementary Note**). No subjects received preoperative treatments, including immunotherapies or molecular targeted therapies. Histopathological specimens were reviewed to confirm that the tumor specimens were histologically consistent with ccRCC (**Supplementary Figs. 14 and 22**). This study was approved by the ethics committee of the Graduate School of Medicine at the University of Tokyo.

**Whole-genome sequencing.** For whole-genome sequencing, genomic DNA was sonicated to generate approximately 400-bp fragments and was analyzed by HiSeq 2000 with the 100-bp paired-end read option according to the manufacturer's protocol.

FASTQ sequences generated by CASAVA 1.8 were aligned to the human reference genome (hg19) using Burrows-Wheeler Aligner (BWA)<sup>44</sup> version 0.5.8. We attempted to realign unmapped or poorly mapped reads using BLAT<sup>45</sup>. For both SNVs and indels, the variant bases found in  $\geq 7$  reads in tumor samples and in  $\leq 1$  (SNVs) or 0 (indels) reads in germline samples were designated as variants. Within noncoding regions, variants found on average in 1% of the total reads in 13 unrelated germline samples were excluded from further analysis owing to the high probability that they represented false positives. Synonymous variants and variants found in either an in-house SNP database constructed from exome sequence data from 98 germline samples, dbSNP131 or the 1000 Genomes Project database were excluded. We also excluded SNVs that were in a tandem repeat region identified using tandem repeats finder<sup>46</sup> and indels that were in RepeatMasker.

To detect structural variations, soft-clipped sequences that could be mapped to unique genomic positions were collected. Structural variation candidates were called if they had  $>4$  supporting read pairs in total and at least 1 read pair from each shore of the breakpoint. Structural variations having a contig sequence that could be aligned to an alternate assembly of the hg19 genome with  $>93\%$  identity were excluded as false positives. Structural variations with a read depth of  $>150$  at either breakpoint were considered to be in a repeat element and were excluded.

**Whole-exome and RNA sequencing.** Whole-exome sequencing was performed using target capture with SureSelect v.4 followed by sequencing as previously described<sup>37</sup>. Mutation calling used the EBcall algorithm<sup>47</sup>. For targeted sequencing, 3 mg of whole-genome DNA was amplified using the REPLI-g kit (Qiagen) and sonicated to generate a peak target size of 200 bp. Captured targets were sequenced using the Illumina HiSeq2000 platform with the 100-bp paired-end read option. A custom bait (SureSelect) library for a panel of eight genes was used for target capture, and high-throughput sequencing was performed using the 100-bp paired-end read option. Libraries for RNA sequencing were generated using the TruSeq RNA Sample Preparation kit (Illumina) and were analyzed using the Illumina HiSeq 2000 platform with 100-bp paired-end reads according to the manufacturer's protocol. Gene fusion detection was performed using Genomon-fusion.

To detect significantly mutated genes, the background mutation rate was calculated for each gene on the basis of data from the current whole-exome sequencing study, taking into consideration the effect of the replication timing of the gene during DNA replication on the background mutation rate as previously described<sup>48,49</sup>. Mutations showing significantly higher mutation frequencies compared to the

corresponding background mutation rate were adopted as significantly mutated genes, with Benjamini-Hochberg correction applied.

**Analysis of significantly mutated pathways.** To detect significantly mutated pathways, each pathway registered in the Kyoto Encyclopedia of Genes and Genomes (KEGG), BioCarta, Reactome, Sigma-Aldrich and Signaling Transduction KE was tested with the PathScan package<sup>50</sup> on the basis of the background mutation rate observed in whole-exome sequencing data. We excluded somatic mutations that were not observed in RNA sequencing because we expected that they would make only a small contribution to pathogenesis. Benjamini-Hochberg correction was applied.

**PCR-based deep sequencing.** To validate somatic mutations and estimate mutant allele frequencies, we conducted deep sequencing using the Illumina MiSeq platform. We randomly selected SNVs and indels called through our pipeline, finding that TPRs were 99% (476/477) for coding SNVs, 99% (93/94) for noncoding SNVs, 96% (29/30) for coding indels and 97% (32/33) for noncoding indels in whole-genome sequencing. In whole-exome sequencing, TPRs were 96% (504/525) for SNVs and 96% (55/57) for indels. Primer sequences are shown in **Supplementary Tables 13 and 14**.

**Microarray analyses.** Global DNA methylation profiles were analyzed using the Infinium HumanMethylation450 BeadChip (Illumina) according to the manufacturer's instructions. To determine DNA methylation profiles, the following filtering steps were adopted to select probes for unsupervised clustering analysis. We first removed probes that were designed for sequences on the X and Y chromosomes. Second, we selected probes with variance ranked in the top 1% of the remaining probes. We then performed unsupervised hierarchical clustering with 3,562 probes, identifying 3 distinct clusters. The  $\beta$  values of 1,672 probes, containing 1,228 genes, that were differentially methylated in the high and low-intermediate groups were represented graphically using a heatmap. Genome-wide analysis of DNA copy number was conducted for 240 tumor-normal specimens using the Affymetrix GeneChip Human Mapping 250K NspI Array according to the manufacturer's protocol. Microarray data were analyzed to determine total and allele-specific copy numbers using CNAG/AsCNAR<sup>51,52</sup>. Significant focal copy number alterations were identified using GISTIC 2.0. Gene expression analysis used 500 ng of total RNA extracted from each tumor ( $n = 101$ ) using the Human Gene Expression 4x44K v2 Microarray (Agilent) according to the manufacturer's instructions. GSEA was performed for both gene expression and DNA methylation using the curated gene sets (c2) acquired from MSigDB.

**Multivariate analysis.** To evaluate the impact of the mutation status of *PBRM1*, *BAP1* and *SETD2* on overall survival and disease-free survival, we performed multivariate analysis of the three genes for an extended cohort of 240 ccRCC cases.

**Immunostaining for HIF-1 $\alpha$ , HIF-2 $\alpha$  and TFE3.** Immunohistochemistry used mouse monoclonal antibody against HIF-1 $\alpha$  (1:300 dilution; clone H1alpha67, NB100-105, Novus Biomedicals) and rabbit polyclonal antibody against HIF-2 $\alpha$  (1:1,000 dilution; NB100-122, Novus Biomedicals). Cases were considered positive for expression when  $>5\%$  of tumor cells showed nuclear immunoreactivity. Expression-positive cases were further classified on the basis of the intensity of nuclear immunoreactivity: 1+, mild; 2+, moderate; 3+, strong. Immunohistochemistry for TFE3 was performed as previously described<sup>53</sup> (sc-5958, Santa Cruz Biotechnology).



**Plasmid construction.** Full-length *TCEB1* cDNA was obtained by PCR amplification of DNA extracted in normal human colon and was cloned adjacent to a sequence encoding three copies of a hemagglutinin (HA) tag at the N terminus of the protein. This construct was subcloned into pMXs-puro<sup>54</sup>, pGCDNsamIRESEGFP<sup>55</sup> and pCI-neo (Promega). cDNA encoding the Tyr79Cys and Ala100Pro mutants was obtained from *in vitro* mutagenesis using wild-type *TCEB1* cDNA as the template and the QuikChange Site-Directed Mutagenesis kit (Stratagene). In the pGCDNsamIRESEGFP-*TCEB1* constructs, four synonymous nucleotide substitutions, c.210A>C (p.Leu70Leu) and c.211\_213TCG>AGC (p.Ser71Ser), were introduced to protect the transcripts from targeting by siRNA designed for endogenous *TCEB1* transcripts using PrimeSTAR HS DNA Polymerase (Takara Bio) according to the manufacturer's protocol. Human *TCEB2* cDNA was obtained with the same method as for *TCEB1* and was cloned into pCI-neo. For *VHL*, *FEM1B*, *TCEB3*, *LRR1* and *SOCS3*, each cDNA was tagged with three copies of sequence encoding a Flag epitope (Flag tag) at its N terminus and was cloned into pCDNA3/Puro<sup>56</sup>.

**Cell culture and gene transfer.** HeLa, HEK 293T and 293gp cells were maintained in DMEM (Gibco) supplemented with 10% FCS and 1% penicillin and streptomycin in a humidified atmosphere with 5% CO<sub>2</sub> or 10% CO<sub>2</sub> at 37 °C. HeLa cells were engineered to stably express wild-type or mutant *TCEB1* or indicated empty vectors (mock) using retrovirus-mediated gene transfer (pMXs-puro-*TCEB1* or pGCDNsamIRESEGFP-*TCEB1*)<sup>37</sup>. HeLa cells transfected with pMXs-puro were subjected to puromycin selection. Cells transduced with pGCDNsamIRESEGFP were sorted for green fluorescent protein (GFP) signal using a flow cytometer (BD FACSAria III, Becton Dickinson). HEK 293T cells were transiently cotransfected with the indicated genes by the calcium phosphate transfection method. Cells were used for experiments after 48 h in culture.

**RNA interference.** Synthetic siRNAs were obtained from Takara Bio (Supplementary Table 7b). HeLa cells were transfected with each siRNA using Lipofectamine 2000 (Invitrogen) according to the manufacturer's instructions. Cells were used for experiments after incubation for 48 h.

**Quantitative RT-PCR.** RNA (500 ng) extracted from the indicated cells using the RNA RNeasy Mini kit (Qiagen) was subjected to reverse transcription using the ReverTra Ace qPCR RT kit (Toyobo) according to the manufacturer's protocol. Quantitative expression levels of mRNA were measured as described previously<sup>37</sup>. Primers used for quantitative RT-PCR are listed in Supplementary Table 7c.

**Antibodies.** Antibodies used for immunoblot analysis are described in Supplementary Table 15. Antibodies were from commercial companies except for antibody against Elongin B<sup>57</sup>.

**Protein extraction and immunoblot analysis.** Cells were lysed in RIPA buffer (Santa Cruz Biotechnology). Lysates were subjected to SDS-PAGE. Proteins were separated and electrophoretically transferred to polyvinylidene difluoride (PVDF) membranes. Membranes were incubated with the indicated antibodies, and proteins were detected using Immobilon Western Chemiluminescent HRP Substrate (Millipore).

**Immunoprecipitation.** Cells transfected with the indicated vectors were lysed. For endogenous VHL stabilization, HeLa cells transfected with pMXs-puro-*TCEB1* were treated with 10 mM MG132 for 6 h before harvesting. HEK 293T cells cotransfected with constructs encoding HA-*TCEB1*, untagged *TCEB2* and Flag-tagged binding proteins were subjected to immunoprecipitation using an antibody to HA or Flag, and immunoblotting was performed as described.

44. Li, H. & Durbin, R. Fast and accurate short read alignment with Burrows-Wheeler transform. *Bioinformatics* **25**, 1754–1760 (2009).
45. Kent, W.J. BLAT—the BLAST-like alignment tool. *Genome Res.* **12**, 656–664 (2002).
46. Benson, G. Tandem repeats finder: a program to analyze DNA sequences. *Nucleic Acids Res.* **27**, 573–580 (1999).
47. Shiraishi, Y. *et al.* An empirical Bayesian framework for somatic mutation detection from cancer genome sequencing data. *Nucleic Acids Res.* **41**, e89 (2013).
48. Hellmann, I. *et al.* Why do human diversity levels vary at a megabase scale? *Genome Res.* **15**, 1222–1231 (2005).
49. Stamatoyannopoulos, J.A. *et al.* Human mutation rate associated with DNA replication timing. *Nat. Genet.* **41**, 393–395 (2009).
50. Wendl, M.C. *et al.* PathScan: a tool for discerning mutational significance in groups of putative cancer genes. *Bioinformatics* **27**, 1595–1602 (2011).
51. Nannya, Y. *et al.* A robust algorithm for copy number detection using high-density oligonucleotide single nucleotide polymorphism genotyping arrays. *Cancer Res.* **65**, 6071–6079 (2005).
52. Yamamoto, G. *et al.* Highly sensitive method for genomewide detection of allelic composition in nonpaired, primary tumor specimens by use of Affymetrix single-nucleotide-polymorphism genotyping microarrays. *Am. J. Hum. Genet.* **81**, 114–126 (2007).
53. Tsuji, K., Ishikawa, Y. & Imamura, T. Technique for differentiating alveolar soft part sarcoma from other tumors in paraffin-embedded tissue: comparison of immunohistochemistry for TFE3 and CD147 and of reverse transcription polymerase chain reaction for *ASPSCR1-TFE3* fusion transcript. *Hum. Pathol.* **43**, 356–363 (2012).
54. Morita, S., Kojima, T. & Kitamura, T. Plat-E: an efficient and stable system for transient packaging of retroviruses. *Gene Ther.* **7**, 1063–1066 (2000).
55. Nabekura, T., Otsu, M., Nagasawa, T., Nakauchi, H. & Onodera, M. Potent vaccine therapy with dendritic cells genetically modified by the gene-silencing-resistant retroviral vector GCDNsap. *Mol. Ther.* **13**, 301–309 (2006).
56. Kamura, T. *et al.* VHL-box and SOCS-box domains determine binding specificity for Cul2-Rbx1 and Cul5-Rbx2 modules of ubiquitin ligases. *Genes Dev.* **18**, 3055–3065 (2004).
57. Garrett, K.P. *et al.* Positive regulation of general transcription factor SIII by a tailed ubiquitin homolog. *Proc. Natl. Acad. Sci. USA* **92**, 7172–7176 (1995).



# Naive and memory human B cells have distinct requirements for STAT3 activation to differentiate into antibody-secreting plasma cells

Elissa K. Deenick,<sup>1,2</sup> Danielle T. Avery,<sup>1</sup> Anna Chan,<sup>1</sup> Lucinda J. Berglund,<sup>1,2,3</sup> Megan L. Ives,<sup>1,2</sup> Leen Moens,<sup>1</sup> Jennifer L. Stoddard,<sup>4</sup> Jacinta Bustamante,<sup>6,7,8</sup> Stephanie Boisson-Dupuis,<sup>6,9</sup> Miyuki Tsumura,<sup>10</sup> Masao Kobayashi,<sup>10</sup> Peter D. Arkwright,<sup>11</sup> Diana Averbuch,<sup>12</sup> Dan Engelhard,<sup>12</sup> Joachim Roesler,<sup>13</sup> Jane Peake,<sup>14</sup> Melanie Wong,<sup>15</sup> Stephen Adelstein,<sup>16</sup> Sharon Choo,<sup>17</sup> Joanne M. Smart,<sup>17</sup> Martyn A. French,<sup>18,19</sup> David A. Fulcher,<sup>3</sup> Matthew C. Cook,<sup>20,21,22</sup> Capucine Picard,<sup>6,7,8</sup> Anne Durandy,<sup>7,8,23</sup> Christoph Klein,<sup>24</sup> Steven M. Holland,<sup>5</sup> Gulbu Uzel,<sup>5</sup> Jean-Laurent Casanova,<sup>6,8,9</sup> Cindy S. Ma,<sup>1,2</sup> and Stuart G. Tangye<sup>1,2</sup>

<sup>1</sup>Immunology and Immunodeficiency Group, Immunology Research Program, Garvan Institute of Medical Research, Darlinghurst, NSW 2010, Australia

<sup>2</sup>St. Vincent's Clinical School, University of New South Wales, Sydney, NSW 2052, Australia

<sup>3</sup>Department of Immunology, Institute of Clinical Pathology and Medical Research, Westmead Hospital, Westmead, NSW 2145, Australia

<sup>4</sup>Clinical Center; and <sup>5</sup>Laboratory of Clinical Infectious Diseases, National Institute of Allergy and Infectious Diseases; National Institutes of Health, Bethesda, MD 20892

<sup>6</sup>Laboratory of Human Genetics of Infectious Diseases, Necker Branch, French Institute of Health and Medical Research (INSERM) U980, Necker Medical School, University Paris Descartes, Paris, 75993 Paris, France

<sup>7</sup>Study Center for Primary Immunodeficiencies, AP-HP, Necker Hospital, 75015 Paris, France

<sup>8</sup>Université Paris Descartes, Institut Imagine, 75015 Paris, France

<sup>9</sup>St. Giles Laboratory of Human Genetics of Infectious Diseases, Rockefeller Branch, The Rockefeller University, New York, NY 10065

<sup>10</sup>Department of Pediatrics, Hiroshima University Graduate School of Biomedical and Health Sciences, Hiroshima 739-0511, Japan

<sup>11</sup>University of Manchester, Royal Manchester Children's Hospital, Manchester M13 9WL, England, UK

<sup>12</sup>Department of Pediatrics and Pediatric Infectious Diseases, Hadassah-Hebrew University Medical Centre, Jerusalem 91120, Israel

<sup>13</sup>Department of Pediatrics, University Clinic Carl Gustav Carus, 01307 Dresden, Germany

<sup>14</sup>Department of Paediatrics and Child Health, Royal Children's Hospital Brisbane, Brisbane, QLD 4029, Australia

<sup>15</sup>Department of Allergy and Immunology, Children's Hospital at Westmead, Westmead, NSW 2145, Australia

<sup>16</sup>Department of Clinical Immunology, Royal Prince Alfred Hospital, Sydney, NSW 2050, Australia

<sup>17</sup>Department of Allergy and Immunology, Royal Children's Hospital Melbourne, Parkville, VIC 3052, Australia

<sup>18</sup>Department of Clinical Immunology, Royal Perth Hospital, Perth, WA 6000, Australia

<sup>19</sup>School of Pathology and Laboratory Medicine, University of Western Australia, Crawley, WA 6009, Australia

<sup>20</sup>Australian National University Medical School and <sup>21</sup>John Curtin School of Medical Research, Australian National University, Canberra, ACT 0200, Australia

<sup>22</sup>Department of Immunology, The Canberra Hospital, Canberra, ACT 2601, Australia

<sup>23</sup>INSERM, U768, Hôpital Necker Enfants-Malades, 75743 Paris, France

<sup>24</sup>Department of Pediatrics, Dr. von Hauner Children's Hospital, Ludwig-Maximilians University Munich, 80337 Munich, Germany

**Long-lived antibody memory is mediated by the combined effects of long-lived plasma cells (PCs) and memory B cells generated in response to T cell-dependent antigens (Ags). IL-10 and IL-21 can activate multiple signaling pathways, including STAT1, STAT3, and STAT5; ERK; PI3K/Akt, and potently promote human B cell differentiation. We previously showed that loss-of-function mutations in *STAT3*, but not *STAT1*, abrogate IL-10- and IL-21-mediated differentiation of human naive B cells into plasmablasts. We report here that, in contrast to naive B cells, *STAT3*-deficient memory B cells responded to these *STAT3*-activating cytokines, differentiating into plasmablasts and secreting high levels of IgM, IgG, and IgA, as well as Ag-specific IgG. This was associated with the induction of the molecular machinery necessary for PC formation. Mutations in *IL21R*, however, abolished IL-21-induced responses of both naive and memory human B cells and compromised memory B cell formation in vivo. These findings reveal a key role for IL-21R/STAT3 signaling in regulating human B cell function. Furthermore, our results indicate that the threshold of *STAT3* activation required for differentiation is lower in memory compared with naive B cells, thereby identifying an intrinsic difference in the mechanism underlying differentiation of naive versus memory B cells.**

E.K. Deenick and D.T. Avery contributed equally to this paper.

## CORRESPONDENCE

Stuart G. Tangye:  
s.tangye@garvan.org.au

Abbreviations used: Ab, antibody; AD-HIES, autosomal-dominant hyper-IgE syndrome; Ag, antigen; PC, plasma cell; Tfh cell, T follicular helper cell.

The Rockefeller University Press \$30.00  
J. Exp. Med. 2013 Vol. 210 No. 12 2739-2753  
www.jem.org/cgi/doi/10.1084/jem.20130323

Supplemental Material can be found at:  
<http://jem.rupress.org/content/suppl/2013/11/08/jem.20130323.DC1.html>

2739



Long-lived immunological memory is mediated by the combined effects of long-lived plasma cells (PCs) and memory B cells generated in response to T-dependent antigens (Ags) and underlies the success of most currently available vaccines (Ahmed and Gray, 1996; Rajewsky, 1996; Tangye and Tarlinton, 2009; Goodnow et al., 2010). PCs reside in survival niches in bone marrow and secondary lymphoid tissues and constantly produce high titers of neutralizing antibodies (Abs; Tangye and Tarlinton, 2009; Tangye, 2011). In contrast, memory B cells recirculate throughout peripheral blood, secondary lymphoid tissues, and bone marrow. Upon reexposure to Ag, they can proliferate and differentiate into Ab-secreting plasmablasts more rapidly than naive cells, thereby replenishing the PC pool and simultaneously expanding the memory cell population (Ahmed and Gray, 1996; Rajewsky, 1996; Tangye and Tarlinton, 2009).

Analysis of gene-targeted mice and humans with monogenic primary immunodeficiencies has identified some of the molecular requirements for memory B cell generation. Thus, mutations in B cell-intrinsic genes (*CD19/CD81*, *CD40*, *IKBKG*, *DOCK8*, and *IL2RG*) or genes expressed by CD4<sup>+</sup> T helper cells (*CD40LG*, *ICOS*, and *SH2D1A* [SAP]) all result in reductions in the frequencies of memory B cells and associated deficiencies in total serum Ig levels or Ag-specific Ab (Tangye and Tarlinton, 2009; Recher et al., 2011; Jabara et al., 2012; Tangye et al., 2012). We also have some understanding of the mechanisms that enable memory B cells to respond more rapidly and vigorously than naive cells to cognate Ag. First, memory B cells are recruited into division significantly earlier and undergo more rounds of division than naive cells (Bernasconi et al., 2002; Tangye et al., 2003a,b; Macallan et al., 2005). Second, memory B cells have higher expression of cell surface receptors, TLRs (TLR7/9/10), CD21, CD27, and TACI, that could enable them to respond more efficiently to co-stimulatory signals (Tangye et al., 1998; Bernasconi et al., 2002, 2003; Darce et al., 2007; Good et al., 2009). Third, memory B cells express heightened levels of CD80 and CD86 (Liu et al., 1995; Tangye et al., 1998; Ellyard et al., 2004; Good et al., 2009), which facilitate soliciting help from T helper cells. Fourth, memory B cells express lower levels of genes that restrict the entry of naive B cells into division, limiting their activation (Good and Tangye, 2007; Horikawa et al., 2007). Lastly, distinct signaling pathways downstream of the B cell receptor expressed by naive (i.e., IgM) or memory (IgG) cells have been identified that preferentially promote responsiveness of memory cells (Martin and Goodnow, 2002; Engels et al., 2009; Davey and Pierce, 2012). However, the requirements for cytokine-mediated regulation of naive and memory B cells remain to be determined.

Human B cell differentiation is regulated by the actions of numerous cytokines, with IL-10 and IL-21, produced by T follicular helper cells (T<sub>fh</sub> cells), being key factors in promoting proliferation, isotype switching, PC differentiation, and secretion of most Ig isotypes by not only naive B cells, but also memory B cells, including both IgM<sup>+</sup> and isotype-switched subsets (Banchereau et al., 1994; Arpin et al., 1997;

Pène et al., 2004; Ettinger et al., 2005; Bryant et al., 2007; Avery et al., 2008a,b). Although the functions of IL-10 and IL-21 on human B cells are similar, the effects of IL-21 exceed those of IL-10 by 10–100-fold (Bryant et al., 2007). The importance of IL-21 to immune regulation has been validated by the recent identification of IL-21R-deficient humans, who exhibit infectious susceptibility to several pathogens (Kotlarz et al., 2013). The predominance of IL-21 in regulating human B cell function over IL-10 is also indicated by the fact that *IL21R* mutations result in poor Ab responses after vaccination (Kotlarz et al., 2013), whereas specific Abs are produced at normal levels in individuals with mutations in *IL10/IL10R* (Kotlarz et al., 2012). IL-10 and IL-21 activate STAT1, STAT3, STAT5, as well as MAPK/ERK and PI3K/Akt pathways (Asao et al., 2001; Zeng et al., 2007; Avery et al., 2008b, 2010; Diehl et al., 2008). Autosomal-dominant hyper-IgE syndrome (AD-HIES) is caused by heterozygous mutations in *STAT3* (Holland et al., 2007; Minegishi et al., 2007; Casanova et al., 2012). These mutations operate in a dominant-negative manner, effectively reducing the level of functional STAT3 by 75%. Loss-of-function mutations in *STAT1* also underlie several immunodeficiency states, such as those characterized by selective susceptibility to infection with environmental mycobacteria and, depending on the nature of the mutation (i.e., dominant/recessive), some viruses (Boisson-Dupuis et al., 2012; Casanova et al., 2012). By examining these patients, we previously found that functional STAT3 deficiency not only severely compromised the generation of memory (i.e., CD27<sup>+</sup>) B cells in vivo, but prevented IL-10- and IL-21-mediated induction of *PRDM1* (Blimp-1 [B lymphocyte induced maturation protein-1]) and *XBPI* (*X-box binding protein 1*) in naive B cells and their subsequent differentiation to the PC lineage in vitro. However, STAT3 mutant (STAT3<sub>MUT</sub>) naive B cells could still acquire expression of *AICDA* (*activation-induced cytidine deaminase*) and undergo IL-21-induced isotype switching in vitro. In contrast, STAT1 was dispensable for human B cell differentiation in vivo and in vitro (Avery et al., 2010).

These findings led us to investigate further the role of STATs in governing human B cell differentiation. We have now discovered that the small number of memory B cells generated in STAT3-deficient patients are unaffected by these mutations; thus, they are capable of differentiating into Ab-secreting cells in response to STAT3-activating cytokines as efficiently as normal memory cells. These findings demonstrate that the threshold of STAT3 activation required for B cell differentiation is significantly lower in memory compared with naive cells. Consequently, limiting amounts of functional STAT3 are sufficient to mediate memory, but not naive, B cell differentiation, thereby revealing an intrinsic difference in the requirements for activating naive versus memory B cells. The memory B cell deficiency in AD-HIES patients likely contributes to impaired Ag-specific Ab responses characteristic of these individuals. Thus, by targeting the residual population of STAT3-deficient memory B cells to respond to IL-21, it may be possible to improve humoral immunity in AD-HIES.

**Table 1.** Characteristics of CD27<sup>-</sup> and CD27<sup>+</sup> B cells in STAT3-deficient individuals

Parameter	CD27 <sup>-</sup> B cells		CD27 <sup>+</sup> B cells	
	Normal	STAT3 <sub>MUT</sub>	Normal	STAT3 <sub>MUT</sub>
% Cells	75.2 ± 2.7	94.9 ± 0.77	24.8 ± 2.7	5.1 ± 0.77
% IgM <sup>+</sup>	87.0 ± 2.2	90.0 ± 2.0	47 ± 3.8	48 ± 3.1
% IgD <sup>+</sup>	88.0 ± 1.9	93.0 ± 1.8	41 ± 2.2	45 ± 2.0
% IgG <sup>+</sup>	3.2 ± 0.45	1.6 ± 0.6 <sup>a</sup>	25 ± 2.1	32 ± 2.8 <sup>a</sup>
% IgG1 <sup>+</sup> (% total IgG <sup>+</sup> cells)	2.3 ± 1.0 (62.1)	0.63 ± 0.24 (40.1)	11 ± 1.7 (51.4)	22 ± 2.8 (72.7) <sup>b</sup>
% IgG2 <sup>+</sup> (% total IgG <sup>+</sup> cells)	0.72 ± 0.14 (19.4)	0.54 ± 0.1 (34.4)	6.7 ± 2.1 (31.3)	3.9 ± 0.9 (12.9)
% IgG3 <sup>+</sup> (% total IgG <sup>+</sup> cells)	0.62 ± 0.15 (16.7)	0.36 ± 0.12 (22.9)	3.6 ± 0.9 (16.8)	4.1 ± 1.1 (13.5)
% IgG4 <sup>+</sup> (% total IgG <sup>+</sup> cells)	0.065 ± 0.02 (1.8)	0.04 ± 0.014 (2.5)	0.11 ± 0.04 (0.5)	0.27 ± 0.08 (0.9)
% IgA <sup>+</sup>	1.2 ± 0.2	0.64 ± 0.15 <sup>a</sup>	17 ± 1.2	8.6 ± 1.1 <sup>c</sup>
% CD23 <sup>+</sup>	62.0 ± 3.9	86.0 ± 3.7 <sup>c</sup>	18 ± 3.9	46 ± 4.7 <sup>c</sup>

Values represent percentage (or absolute number for CD4<sup>+</sup>CXCR5<sup>+</sup> T cells) of cells expressing the indicated surface molecule; each value represents the mean ± SEM; normal donors: *n* = 8–24; STAT3 patients: *n* = 9–27. P-values were determined by Student's *t* test, comparing normal with STAT3<sub>MUT</sub> B cells.

<sup>a</sup>P < 0.05.

<sup>b</sup>P < 0.01.

<sup>c</sup>P < 0.001.

## RESULTS

### STAT3<sub>MUT</sub> CD27<sup>+</sup> B cells phenotypically resemble normal memory B cells

The population of circulating CD27<sup>+</sup> memory B cells is significantly reduced in STAT3-deficient patients (*n* = 27) compared with normal donors (Table 1; Avery et al., 2010). In contrast, the frequency of memory B cells in STAT1-deficient individuals is comparable with normal donors (i.e., 24.4 ± 6.1%; *n* = 9). Although it is generally accepted that CD27 is expressed on human memory B cells (Tangye and Tarlinton, 2009), recent studies have suggested that B1 cells (Griffin et al., 2011) and some bone marrow progenitor B cells (Nilsson et al., 2005) are also CD27<sup>+</sup>. Conversely, a small proportion of memory B cells lack CD27 (Tangye and Tarlinton, 2009). Thus, it was important to establish the nature of the residual population of CD27<sup>+</sup> B cells in STAT3<sub>MUT</sub> patients.

The size and granularity of CD27<sup>-</sup> and CD27<sup>+</sup> B cells were determined by flow cytometry. This demonstrated that CD27<sup>+</sup> B cells from both normal donors and STAT3<sub>MUT</sub> patients were significantly larger and more granular than corresponding CD27<sup>-</sup> B cells. However, these morphological features were not significantly different between cells from normal donors and STAT3<sub>MUT</sub> patients (Fig. 1, A–C).

We next examined a series of surface receptors that are differentially expressed by human naive and memory B cells (Liu et al., 1995; Tangye et al., 1998; Ellyard et al., 2004; Good et al., 2009). CD24, CD80, CD95, and TACI were significantly higher on CD27<sup>+</sup> B cells from normal donors than on corresponding CD27<sup>-</sup> B cells (Fig. 1, A and C). CD86 also tended to be higher on normal CD27<sup>+</sup> versus CD27<sup>-</sup> B cells (Fig. 1, A and C). The same pattern was seen for samples from STAT3<sub>MUT</sub> patients, with CD80, CD86, CD95, and TACI being significantly higher on CD27<sup>+</sup> than on CD27<sup>-</sup> B cells (Fig. 1, B and C). In contrast to these molecules, CD23 is present on normal naive B cells but is

significantly down-regulated on normal memory B cells (Fig. 1, A and C; and Table 1). Interestingly, CD23 expression was dysregulated on STAT3<sub>MUT</sub> B cells inasmuch as its level exceeded that on normal naive B cells by >10-fold, whereas it was detected on a substantial proportion of STAT3<sub>MUT</sub> memory B cells (Fig. 1, B and C; and Table 1).

We also determined expression of Ig isotypes by CD27<sup>-</sup> and CD27<sup>+</sup> B cells from normal and STAT3-deficient individuals. Approximately ~90% of CD27<sup>-</sup> B cells and ~40–50% of CD27<sup>+</sup> B cells from normal and STAT3-deficient individuals expressed IgM and IgD, with the remaining memory B cells expressing predominantly IgG or IgA (Table 1). Although the proportion of STAT3<sub>MUT</sub> CD27<sup>+</sup> B cells that expressed IgG was greater than that observed for normal CD27<sup>+</sup> B cells (Table 1), the distribution of IgG subclasses within the CD27<sup>-</sup> and CD27<sup>+</sup> B cell subsets was comparable, with IgG1 being preferentially expressed by both CD27<sup>-</sup> and CD27<sup>+</sup> normal and STAT3<sub>MUT</sub> B cells (Table 1). Furthermore, we did not detect an enrichment of B1 cells, based on cells with a CD20<sup>+</sup>CD43<sup>+</sup>CD27<sup>+</sup> phenotype, in STAT3<sub>MUT</sub> individuals compared with healthy donors (not depicted). Collectively, these findings confirm there is a significant contraction of the memory B cell compartment in AD-HIES and provide evidence that the small population of CD27<sup>+</sup> B cells in STAT3<sub>MUT</sub> individuals are indeed memory B cells (Table 1).

### IL-21 activates STAT1, STAT3, and STAT5 in naive and memory B cells

IL-21 has been reported to activate multiple signaling pathways in different cell types (Asao et al., 2001; Zeng et al., 2007; Diehl et al., 2008). To determine whether different subsets of human B cells used similar signaling pathways downstream of the IL-21 receptor, we examined phosphorylation of STAT proteins in normal naive, IgM memory, and

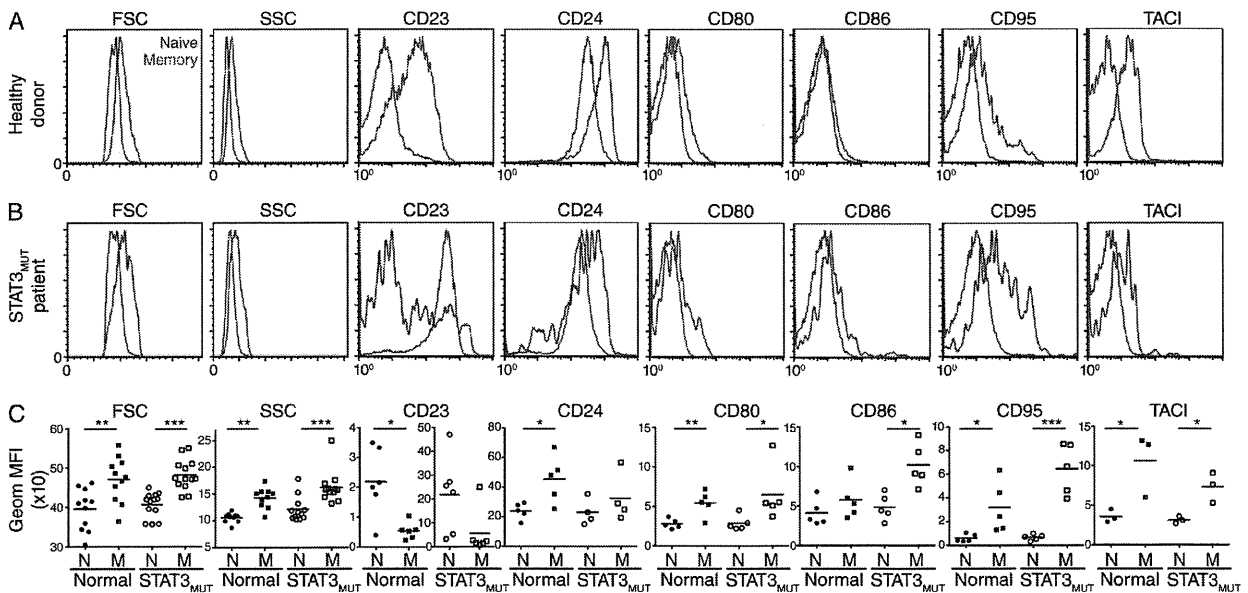


**Figure 1. Morphology and phenotype of CD27<sup>+</sup> B cells in STAT3<sub>MUT</sub> individuals resemble normal memory B cells.** (A–C) PBMCs from normal donors and patients with AD-HIES caused by mutations in *STAT3* were stained with mAbs specific for CD20, CD27, and CD23, CD24, CD80, CD86, CD95, or TAC1. The forward scatter (FSC) and 90° light/side scatter (SSC) and surface expression of the indicated molecules on CD27<sup>−</sup> (naive) and CD27<sup>+</sup> (memory) B cells were determined. The histograms in A and B are from a representative normal donor and patient, respectively, whereas the graphs in C depict the geometric mean fluorescence intensity (MFI) of each of the indicated cellular features for CD27<sup>−</sup> naive (N) and CD27<sup>+</sup> memory (M) B cells from 3–12 normal donors and STAT3<sub>MUT</sub> patients. Each value represents an individual donor or patient; the horizontal lines correspond to the mean. Because of the large difference in the level of expression of CD23 on normal versus STAT3<sub>MUT</sub> naive and memory B cells, individual graphs are depicted for normal and patient B cell subsets. \*, P < 0.05; \*\*, P < 0.01; \*\*\*, P < 0.001.

isotype-switched memory B cells in response to IL-21. Phosphorylation of STAT1, STAT3, and STAT5 was greater in naive B cells than in memory B cells; however, STAT1 and STAT3 were both clearly activated by IL-21 in both IgM-expressing and Ig-switched memory B cell subsets (Fig. 2, A and B). In contrast to these STATs, IL-21 had minimal, if any, effect on phosphorylation of STAT4 or STAT6 (Fig. 2 A). Although IL-21 has been reported to activate ERK and AKT (Zeng et al., 2007), we observed no ERK or AKT phosphorylation in response to IL-21 in naive or memory B cells (Fig. 2, C and D). These results demonstrate that IL-21R signaling activates similar pathways in human naive and memory B cells, predominantly STAT1, STAT3, and STAT5.

#### Mutations in *STAT3* impair the response of naive, but not memory, B cells to the stimulatory effects of IL-10 and IL-21

STAT3 is required for some, but not all, aspects of naive B cell differentiation. For instance, isotype switching was intact in STAT3<sub>MUT</sub> B cells, as indicated by the detection of circulating IgG<sup>+</sup> and IgA<sup>+</sup> B cells in AD-HIES patients ex vivo (Table 1) and the ability of their naive B cells to up-regulate *AICDA* and switch to IgG in response to IL-21 in vitro (Avery et al., 2010). Consistent with intact *AICDA* expression in STAT3<sub>MUT</sub> naive B cells in vitro, somatic hypermutation was comparable in normal and STAT3<sub>MUT</sub> memory B cells (Avery et al., 2010). These observations lead us to question whether there were also

differences between naive and memory B cells in their requirement for STAT3 function to respond to cytokines such as IL-10 and IL-21, which are well known for their abilities to induce human B cell differentiation (Banchereau et al., 1994; Arpin et al., 1997; Pène et al., 2004; Ettinger et al., 2005; Bryant et al., 2007; Avery et al., 2008a,b).

Naive and memory B cells isolated from normal donors or STAT3<sub>MUT</sub> or STAT1<sub>MUT</sub> patients were cultured with CD40L alone or together with IL-21, and Ig secretion was determined after 10–12 d. Because of the limited numbers of memory cells recovered from STAT3<sub>MUT</sub> patients, we could only culture ~5,000 sorted B cells/well. Under these conditions, IL-21 potently promoted secretion of IgM and induced production of IgG and IgA by normal and STAT1<sub>MUT</sub> naive B cells (Fig. 3 A and Table 2). IL-21 substantially increased production of IgM, IgG, and IgA by CD40L-stimulated memory B cells from normal donors and STAT1-deficient individuals; however, the response of STAT1<sub>MUT</sub> memory B cells was significantly less (approximately fourfold) than that of normal memory cells (Fig. 3 B and Table 2). Ig secretion by STAT3<sub>MUT</sub> naive B cells in response to IL-21 was ~30-fold less than normal naive cells (Fig. 3 A and Table 2; P < 0.001). In distinct contrast, Ig secretion by IL-21-stimulated STAT3<sub>MUT</sub> memory B cells (either total memory cells [Fig. 3 B and Table 2] or IgM<sup>+</sup> and switched subsets [not depicted]) was largely comparable with normal memory B cells,

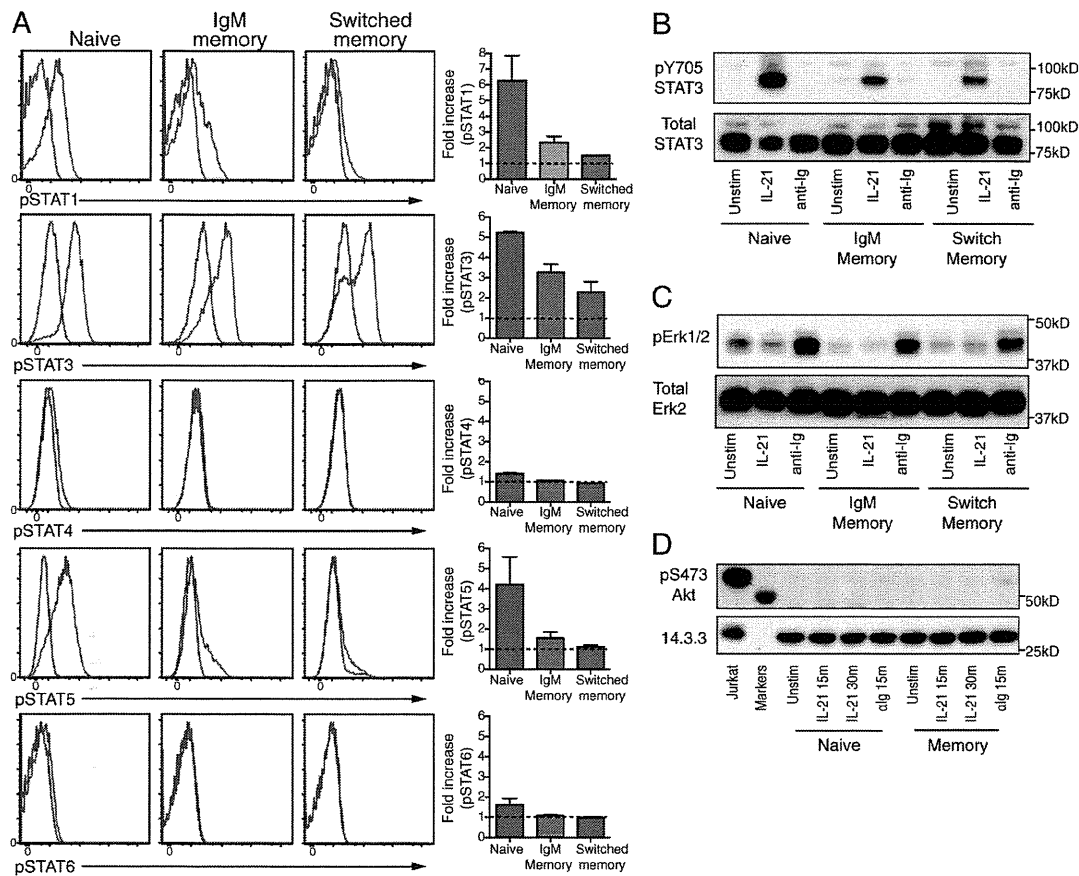


**Figure 2.** IL-21 induces activation of STAT1, STAT3, and STAT5 in human naive and memory B cells. Human naive, IgM memory and isotype-switched memory, or total memory, B cells were sort-purified from normal donor spleens. (A) These B cell subsets were cultured for ~18 h with anti-Ig, rested, and then cultured in the absence (red histograms) or presence (blue histograms) of IL-21 for 30 min. Phosphorylation of STAT1, STAT3, STAT4, STAT5, and STAT6 was determined by intracellular staining. Histograms on the left show representative staining in naive and memory B cells. Right panels plot increase in mean fluorescence intensity of pSTATs in naive, IgM memory, and isotype-switched memory B cells cultured with IL-21; response of unstimulated cells were normalized to a value of 1.0. These values represent the mean  $\pm$  SEM of two independent experiments using B cells from different donor spleens. Identical results were obtained when the B cell subsets were prestimulated with CD40L/anti-Ig. (B–D) Human B cell subsets were cultured for ~18 h with anti-Ig, rested, and then left unstimulated or stimulated with IL-21 or anti-Ig for 15–30 min. Cells lysates were prepared and subjected to SDS-PAGE and Western blotting to detect phosphorylated or total STAT3 (B), phosphorylated or total ERK (C), or phosphorylated AKT or 14.3.3 as a loading control (D). B–D are representative of three to four similar experiments.

with the only significant difference (less than twofold) being noted for the levels of IgM secreted by normal versus STAT3<sub>MUT</sub> memory B cells (Table 2). Furthermore, both IgM memory (i.e., IgM<sup>+</sup>CD27<sup>+</sup>) and switched (IgM/D<sup>-</sup>CD27<sup>+</sup>) memory cells from STAT3-deficient patients could respond to the stimulatory effects of IL-10 (not depicted).

The inability of STAT3<sub>MUT</sub> naive B cells to respond to IL-21 did not reflect a general impairment in differentiation because these cells produced IgM after stimulation with CD40L plus CpG (Fig. 3 C) and up-regulated expression of *AICDA* (Fig. 3 E) and Ig  $\epsilon$  germline transcripts, a precursor to producing mature IgE (Geha et al., 2003), in response to CD40L/IL-4 (Fig. 3 F) as efficiently as normal naive B cells. Consistent with the intact response of STAT3<sub>MUT</sub> memory

B cells to CD40L together with IL-10 or IL-21 (Fig. 3 B, Table 2, and not depicted), these cells also exhibited normal responses to stimulation with CD40L/CpG (Fig. 3 D) or CD40L/IL-4 (Fig. 3, E and F). Because many facets of lymphocyte differentiation are linked to cell division (Hodgkin et al., 1996; Deenick et al., 1999; Tangye et al., 2003a,b; Avery et al., 2005, 2008a), we also assessed the proliferative potential of STAT3<sub>MUT</sub> naive and memory B cells. IL-21 enhanced proliferation of both normal and STAT3<sub>MUT</sub> naive B cells over that induced by CD40L alone, yet the response of STAT3<sub>MUT</sub> naive B cells was approximately threefold less than that of normal B cells (Fig. 3 G). Consistent with the differential dependency on STAT3 function for IL-21-induced Ig secretion by naive versus memory B cells, STAT3<sub>MUT</sub> memory

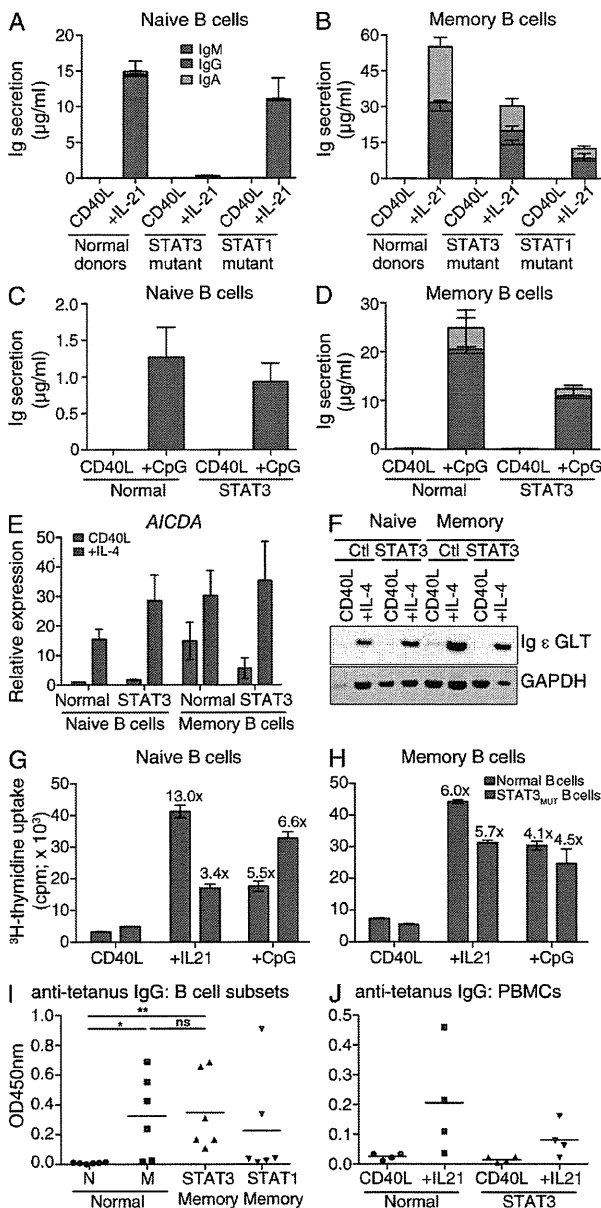


**Figure 3. STAT3-deficient memory B cells differentiate into Ab-secreting cells in response to IL-21.** (A–D) Naive (CD20<sup>+</sup>CD10<sup>-</sup>CD27<sup>-</sup>IgG<sup>-</sup>) and memory (CD20<sup>+</sup>CD10<sup>-</sup>CD27<sup>+</sup>) B cells were sort-purified from normal donors (A and B,  $n = 16$ ; C and D,  $n = 7$ ), STAT3<sup>MUT</sup> patients (A and B,  $n = 8$ ; C and D,  $n = 7$ ), or STAT1<sup>MUT</sup> patients ( $n = 6$ ), and then cultured with CD40L alone or together with IL-21 (A and B) or CpG (C and D). The levels of secreted IgM, IgG, and IgA were determined by ELISA after 10–12 d. The columns represent the mean  $\pm$  SEM of experiments performed using naive B cells from 7–16 normal donors, 7–8 STAT3<sup>MUT</sup> patients, or 6 STAT1<sup>MUT</sup> patients. (E and F) Naive and memory B cells were sort-purified from normal donors or STAT3<sup>MUT</sup> patients and then cultured with CD40L alone or together with IL-4. Expression of *AICDA* (E) and Ig  $\epsilon$  germline transcript (GLT; F) was determined by qPCR and PCR, respectively. The graphs in E represent the mean  $\pm$  SEM of three experiments using B cells from different donors or patients. The gel depicted in F is representative of experiments

B cells proliferated to a similar extent as normal memory B cells in response to IL-21 (Fig. 3 H). Not surprisingly, CD40L/CpG induced comparable proliferation in STAT3-sufficient and -deficient naive and memory B cells (Fig. 3, G and H). Thus, impaired proliferation of naive STAT3<sup>MUT</sup> B cells to IL-21 correlates with poor differentiation of these cells to plasmablasts under these culture conditions. However, naive STAT3<sup>MUT</sup> B cells do undergo some proliferation to IL-21 (Fig. 3 G; Avery et al., 2010), indicating that the block in differentiation is not simply caused by *STAT3* mutations abrogating cell division.

### The memory cell pool in STAT3-deficient individuals contains Ag-specific B cells

Although the total levels of Ig produced by STAT3<sup>MUT</sup> memory B cells in response to STAT3 cytokines were normal, it was unknown whether these B cells could contribute to an Ag-specific Ab response. To address this, we quantified the relative amounts of antitetanus IgG produced by B cells from normal donors or STAT3<sup>MUT</sup> or STAT1<sup>MUT</sup> patients after in vitro culture with CD40L/IL-21. As expected, the levels of antitetanus IgG produced by normal naive B cells were very low/undetectable, whereas memory cells from most normal donors produced significantly higher amounts of tetanus-specific IgG (Fig. 3 I). Importantly, STAT3<sup>MUT</sup> memory B cells from all patients tested produced significantly higher amounts of tetanus-specific IgG than normal naive B cells (Fig. 3 I). Memory B cells from some STAT1<sup>MUT</sup> patients exhibited a lower response than others, but in general this exceeded that of normal naive B cells and, on average, approximated that of normal and STAT3<sup>MUT</sup> memory B cells (Fig. 3 I). We also assessed production of antitetanus IgG in cultures of total PBMCs from normal donors and STAT3<sup>MUT</sup> individuals that had been stimulated with CD40L and IL-21. On average, normal PBMCs produced approximately threefold higher levels of antitetanus IgG than did STAT3<sup>MUT</sup> PBMCs (Fig. 3 J). However, there are several caveats to screening PBMCs, rather than purified B cells, for the production of Ag-specific Ab.

performed using B cells from two to three different donors or patients. (G and H) Naive and memory B cells were sort-purified from a single normal donor or STAT3<sup>MUT</sup> patient and then cultured with CD40L alone or together with IL-21 or CpG. Proliferation was assessed after 5 d by determining incorporation of [<sup>3</sup>H]thymidine during the last 18 h of culture. The graphs are the mean  $\pm$  SEM of replicate cultures of naive or memory B cells from one normal donor or one STAT3<sup>MUT</sup> patient. The annotated values indicate the fold increase in proliferation of normal or STAT3<sup>MUT</sup> naive or memory B cells cultured with CD40L/IL-21 or CD40L/CpG over that induced by CD40L alone. (I and J) Normal naive (N) or normal, STAT3<sup>MUT</sup>, or STAT1<sup>MUT</sup> memory (M) B cells ( $n = 6$ ; I) or total PBMCs from normal donors or STAT3<sup>MUT</sup> patients ( $n = 4$ ; J) were cultured with CD40L and IL-21 for 10–12 d. The levels of antitetanus IgG in culture supernatants were determined by ELISA using immobilized tetanus toxoid as solid phase Ag. Each symbol represents the response of B cells from an individual control or patient; the horizontal bars represent means. ns, no significant; \*,  $P < 0.05$ ; \*\*,  $P < 0.01$ .

**Table 2.** Ig secretion by IL-21-stimulated normal, STAT3<sub>MUT</sub>, and STAT1<sub>MUT</sub> naive and memory B cells

Cell type and culture	Ig secretion								
	IgM			IgG			IgA		
	Normal	STAT3 <sub>MUT</sub>	STAT1 <sub>MUT</sub>	Normal	STAT3 <sub>MUT</sub>	STAT1 <sub>MUT</sub>	Normal	STAT3 <sub>MUT</sub>	STAT1 <sub>MUT</sub>
ng/ml	ng/ml	ng/ml	ng/ml	ng/ml	ng/ml	ng/ml	ng/ml	ng/ml	
<b>Naive B cells</b>									
CD40L	2.0 ± 1.0	5.0 ± 2.4 <sup>a</sup>	<0.1 <sup>a</sup>	<1	<1 <sup>a</sup>	<1 <sup>a</sup>	<1	<1 <sup>a</sup>	<1 <sup>a</sup>
+IL-21	14,640 ± 2,021	444 ± 177 <sup>d</sup>	10,801 ± 3,183 <sup>a</sup>	267 ± 80	7.3 ± 2.7 <sup>b</sup>	86 ± 40 <sup>a</sup>	365 ± 106	4.6 ± 2.6 <sup>b</sup>	174 ± 40 <sup>a</sup>
<b>Memory B cells</b>									
CD40L	166 ± 51	100 ± 25 <sup>a</sup>	2.5 ± 2.5 <sup>a</sup>	6.1 ± 1.4	11.8 ± 4.7 <sup>a</sup>	0.2 ± 0.14 <sup>a</sup>	21.3 ± 6.1	26.2 ± 10.6 <sup>a</sup>	<1 <sup>a</sup>
+IL-21	29,389 ± 4,107	15,214 ± 1,905 <sup>b</sup>	7,396 ± 3,097 <sup>d</sup>	4,202 ± 1,122	5,651 ± 1,743 <sup>a</sup>	953 ± 195 <sup>a</sup>	25,208 ± 4,134	13,330 ± 4,027 <sup>a</sup>	4,265 ± 989 <sup>c</sup>

Naive and memory B cells were sort-purified from normal healthy donors ( $n = 17$ ), STAT3<sub>MUT</sub> patients ( $n = 8$ ), or STAT1<sub>MUT</sub> patients ( $n = 6$ ) and then cultured with CD40L alone or together with IL-21. The levels of secreted IgM, IgG, and IgA were determined by ELISA after 10–12 d. The values represent the mean ± SEM from the indicated number of donors/patients and correspond to the data depicted in Fig. 3 (A and B). Statistical analyses were performed using one-way ANOVA; differences are indicated for normal donors compared with STAT3<sub>MUT</sub> or STAT1<sub>MUT</sub> B cells.

<sup>a</sup>Not significant.

<sup>b</sup>P < 0.01.

<sup>c</sup>P < 0.001.

<sup>d</sup>P < 0.0001.

First, there is substantial variability in the frequencies of B cells within the population of all PBMCs, as well as in the proportion of B cells that are memory cells. Indeed, there is a strong correlation between the frequency of memory B cells and production of antitetanus IgG in vitro (not depicted). Second, the addition of CD40L to cultures of PBMCs will activate myeloid cells (monocytes, macrophages, and DCs) to secrete molecules such as BAFF and APRIL (Litinskiy et al., 2002; Craxton et al., 2003), which can preferentially promote differentiation and Ig secretion by human memory B cells presumably in a STAT3-independent manner (Avery et al., 2003). Even taking these into account, it is clear that STAT3-deficient individuals are capable of generating Ag-specific Ab responses and that these Ag-specific cells reside within the residual subset of CD27<sup>+</sup> B cells. This further substantiates that these cells are indeed memory B cells and are likely to contribute to Ag-specific Ab responses in vivo.

#### STAT1 deficiency does not affect the early differentiation of memory B cells into Ig-secreting plasmablasts

The accumulated levels of Ig secreted by STAT1<sub>MUT</sub> memory B cells were 2.5–5-fold less than those by normal memory cells (Fig. 3 B and Table 2). To determine whether this reflected a quantitative defect in generating Ab-secreting cells from STAT1<sub>MUT</sub> memory B cells, we performed kinetic analyses of plasmablast formation and Ig secretion by normal and STAT1<sub>MUT</sub> naive and memory B cells that had been stimulated with CD40L alone or together with IL-21. CD40L alone resulted in <0.5% of normal and STAT1<sub>MUT</sub> naive B cells and ~1–3% of memory B cells acquiring a CD38<sup>hi</sup>CD27<sup>hi</sup> phenotype, which corresponds to plasmablasts (Fig. 4, A, B, D, and E; Avery et al., 2005). Addition of IL-21 had minimal

effect on naive B cell differentiation, in terms of the frequency of plasmablasts and Ig secretion, after 4 d of culture (Fig. 4, A–C); however, a substantial proportion of memory B cells had differentiated to become Ig-secreting plasmablasts at this time (Fig. 4, D–F). The rate of plasmablast formation from naive and memory B cells increased after 5.5 d and tended to plateau or decline at later times (7 d; Fig. 4, B and E). Co-incident with this was a dramatic increase in Ig secretion by both naive and memory B cells between 4 and 5.5 d of in vitro culture (Fig. 4, C and F). The rate of formation of plasmablasts and Ig secretion by IL-21-stimulated naive and memory B cells was not affected by STAT1 mutations (Fig. 4). Collectively, these results suggested that STAT1<sub>MUT</sub> memory B cells could initially generate normal numbers of functional plasmablasts. However, in contrast to this normal rate of differentiation of STAT1<sub>MUT</sub> memory B cells between days 4 and 7 of culture (Fig. 4, D–F), Ig secretion by these cells after 11 d of culture was consistently less than that by normal memory B cells (Fig. 3 B and Table 2). Thus, STAT1 may play a role in sustaining Ig secretion by differentiated memory B cells.

#### Commitment of memory B cells to the PC lineage is unaffected by mutations in STAT1 or STAT3

The differentiation of human and mouse B cells into PCs is regulated by the coordinated actions of several transcription factors. PAX5 is down-regulated in activated B cells, thereby relieving PAX5-mediated repression of Blimp-1, resulting in Blimp-1 expression. Although Blimp-1 is not required for initial commitment to the PC lineage, it is indispensable for the generation of terminally differentiated PCs. Other transcription factors, XBP-1 and IRF4 (interferon-induced regulatory



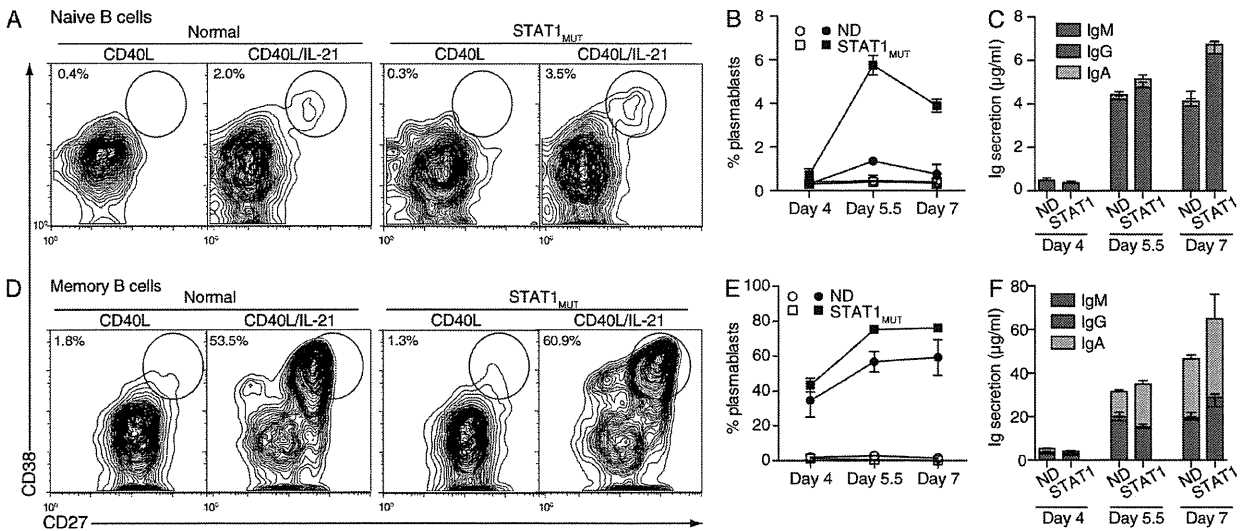


**Figure 4.** *STAT1* mutations do not affect the generation of plasmablasts but impair sustained Ig secretion. (A–F) Naive (A–C) and memory (D–F) B cells were sort-purified from normal donors or *STAT1*<sub>MUT</sub> patients and then cultured ( $25 \times 10^3$ /well/100  $\mu$ l) with CD40L alone (open symbols in B and E) or together with IL-21 (closed symbols in B and E). The generation of plasmablasts, defined as cells acquiring a CD38<sup>hi</sup>CD27<sup>hi</sup> phenotype (A, B, D, and E), as well as secretion of IgM, IgG, and IgA (C and F), was determined after 4, 5.5, and 7 d. The contour plots (A and D) are representative of plasmablasts detected after 5 d of culture. The graphs depicting Ig secretion are from cultures of CD40L/IL-21-stimulated B cells. The values represent the mean ( $\pm$ SEM for B, C, E, and F) of experiments using cells from two normal donors and two *STAT1*<sub>MUT</sub> patients. Similar results were obtained in a second independent experiment.

factor-4), are also involved in PC differentiation (Nutt et al., 2011). A key mechanism by which IL-21 mediates differentiation of naive B cells into PCs is by modulating expression of these transcription factors. Thus, naive B cells lose *PAX5* and acquire *Blimp-1* and *XBP-1* in response to IL-21 in vitro (Ettinger et al., 2005; Bryant et al., 2007).

Our finding that *STAT3*<sub>MUT</sub> memory, but not naive, B cells were capable of secreting near-normal levels of Ig in response to IL-21 (Fig. 3 and Table 2) led us to investigate transcriptional changes in normal and *STAT3*<sub>MUT</sub> naive and memory B cells after stimulation with IL-21. We also examined *STAT1*<sub>MUT</sub> naive and memory B cells as the latter had some defects in secreting normal levels of Ig (Fig. 3 and Table 2). Addition of IL-21 to cultures of B cells from normal donors resulted in the down-regulation of *PAX5* and up-regulation of *PRDM1* and *XBP1* in naive and memory B cells (Fig. 5, A and B). *PRDM1* and *XBP1* were substantially higher, and *PAX5* much lower, in memory versus naive cells (Fig. 5, A and B). Furthermore, although IL-21 had no detectable effect on *IRF4* expression in normal naive B cells (Fig. 5 A), it induced an approximately threefold increase in *IRF4* in normal memory B cells (Fig. 5 B). These differences likely contribute to memory B cells secreting 10–20-fold more Ig than naive cells (Figs. 3 and 4 and Table 2).

*STAT1*<sub>MUT</sub> naive and memory B cells modulated expression of *PAX5*, *PRDM1*, *XBP1*, and *IRF4* in a manner indistinguishable from normal B cells (Fig. 5, A and B), consistent with normal Ig secretion during short-term cultures (Fig. 4, C and F). However, *STAT3*<sub>MUT</sub> B cells revealed marked

differences in the behavior of naive and memory cells. Although naive *STAT3*<sub>MUT</sub> B cells down-regulated *PAX5* in response to IL-21, they failed to up-regulate *PRDM1* and *XBP1* (Fig. 5 A). In stark contrast, IL-21-mediated induction of *PRDM1*, *XBP1*, and *IRF4* in *STAT3*<sub>MUT</sub> memory B cells was intact (Fig. 5 B), mirroring the ability of these cells to secrete large amounts of Ig in response to IL-21 (Fig. 3 B). Induction of *AICDA* in *STAT3*<sub>MUT</sub> naive B cells by IL-21 was comparable with normal and *STAT1*<sub>MUT</sub> naive B cells (Fig. 5 A), further demonstrating that *STAT3*<sub>MUT</sub> naive B cells can respond to IL-21 under the culture conditions used here. In contrast to naive B cells, IL-21 reduced *AICDA* expression in memory B cells from all individuals compared with stimulation with CD40L alone (Fig. 5 B). This is probably a result of memory B cells expressing much higher levels of *PRDM1* (Fig. 5 B), which directly represses *AICDA* (Nutt et al., 2011). Thus, differentiation of naive and memory B cells into Ab-secreting cells, as determined both at the cellular and molecular level, exhibit distinct sensitivity to mutations in *STAT3*.

#### Memory cells exhibit greater sensitivity to the stimulatory effects of *STAT3*-activating cytokines IL-21 and IL-10

One possible explanation for this differential susceptibility to mutations in *STAT3* would be that in memory B cells IL-21 activates an alternate *STAT3*-independent signaling pathway. However, we observed little activation of pathways other than *STAT1* and *STAT3* in memory B cells (Fig. 2). An alternative possibility was that memory B cells expressed higher levels of *STAT3* or were enriched for expression of the wild-type

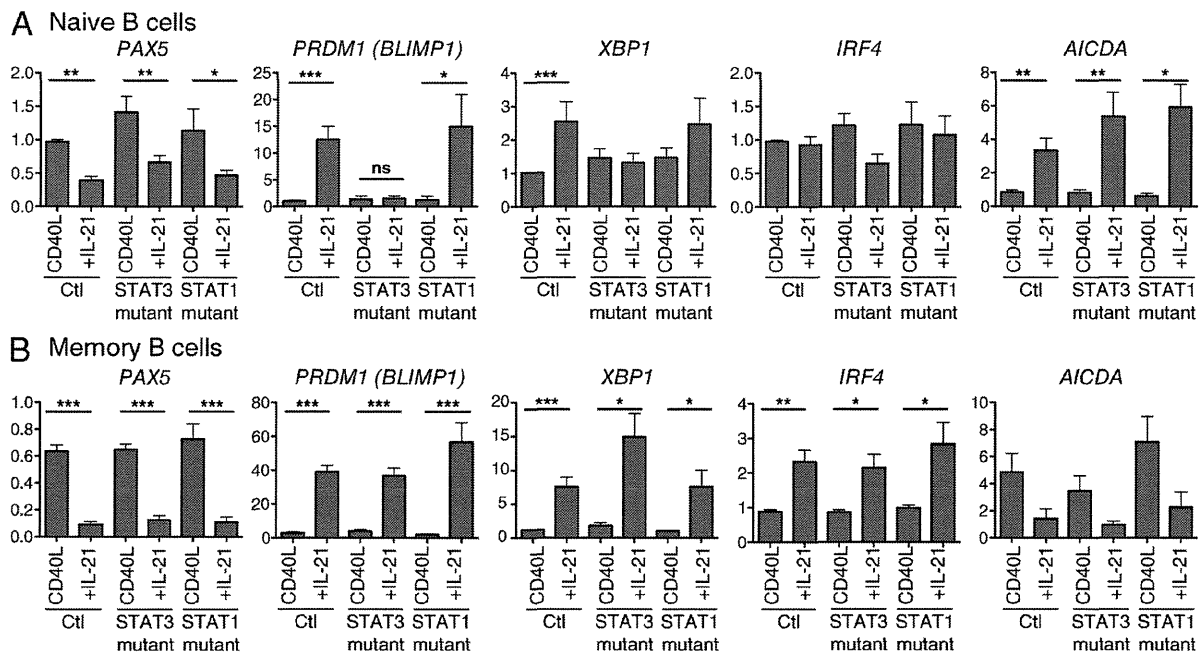


**Figure 5. Induction of the PC transcriptional program is intact in IL-21-stimulated STAT3<sub>MUT</sub> memory B cells.** (A and B) Naive (CD20<sup>+</sup>CD10<sup>-</sup>CD27<sup>-</sup>IgG<sup>-</sup>; A) and memory (CD20<sup>+</sup>CD10<sup>-</sup>CD27<sup>+</sup>; B) B cells were sort-purified from normal donor controls (Ctl;  $n = 10$  [or 7 for *AICDA*]), STAT3<sub>MUT</sub> patients ( $n = 5$ ), or STAT1<sub>MUT</sub> patients ( $n = 4$ ) and then cultured with CD40L alone or together with IL-21 (+IL-21) for 5 d. Expression of *PAX5*, *PRDM1*, *XBP1*, *IRF4*, and *AICDA* was determined by qPCR. The columns represent the mean  $\pm$  SEM of experiments performed using naive B cells from 7–10 normal donors, 5 STAT3<sub>MUT</sub> patients, or 4 STAT1<sub>MUT</sub> patients. Levels of expression are relative to the amount of *GAPDH*. ns, not significant; \*,  $P < 0.05$ ; \*\*,  $P < 0.01$ ; \*\*\*,  $P < 0.001$ .

*STAT3* allele compared with naive B cells. Yet we found that naive and memory B cells from normal donors or AD-HIES patients expressed comparable levels of *STAT3* both ex vivo and after in vitro culture (not depicted) and that the mutant allele still accounted for  $\sim 50\%$  of total *STAT3* that was expressed by memory B cells (not depicted). A final explanation for the differential effects of *STAT3* deficiency on the function of naive versus memory B cells derives from the heterozygous nature of the *STAT3* mutations and the fact that *STATs* exert their effect as dimers. This predicts that the mutant allele acts in a dominant-negative manner, thereby inhibiting the function of up to 75% of *STAT3* dimers and leaving only 25% intact (Holland et al., 2007; Minegishi et al., 2007). Thus, the differential sensitivity of naive and memory B cells to *STAT3* mutations may reflect an increased responsiveness of memory cells to *STAT3* action such that the residual wild-type *STAT3* dimers in STAT3<sub>MUT</sub> memory, but not naive, B cells are sufficient to render these cells responsive to the effects of *STAT3*-activating cytokines. To test whether there are differences in the threshold of activation of naive and memory B cells, these B cell subsets were purified from normal donor spleens and cultured with CD40L and increasing concentrations of IL-21 or IL-10, and induction of expression of *PRDM1* and *XBP1* was determined after 4 d. The concentrations of IL-21 (Fig. 6 A, left) and IL-10 (Fig. 6 B, left) required to induce *PRDM1* in naive B cells

(i.e., 10 ng/ml IL-21 and 100 U/ml IL-10) were at least five times higher than those required for induction in memory B cells (i.e., 2 ng/ml IL-21 and 20 U/ml IL-10). Furthermore, these cytokines induced *PRDM1* in memory B cells at levels that exceeded those in naive B cells by two- to five-fold (Fig. 6, A and B, left). Induction of *XBP1* followed a similar pattern, with expression being detected in memory B cells at much reduced cytokine concentrations than in naive B cells and memory B cells expressing substantially more *XBP1* than naive B cells (Fig. 6, A and B, right). Collectively, these results demonstrate that memory B cells have greater sensitivity to the stimulatory effects of these *STAT3*-activating cytokines, especially when present at limiting concentrations. Thus, it is likely that the small percentage of wild-type *STAT3* dimers that can form in STAT3<sub>MUT</sub> memory B cells are sufficient to integrate signals provided by IL-10 and IL-21 to facilitate the differentiation of memory B cells into Ig-secreting plasmablasts.

#### Loss-of-function mutations in *IL21R* abolishes responses of naive and memory B cells to IL-21

To establish that the differences in responses of naive and memory STAT3<sub>MUT</sub> B cells to IL-21 involved direct signaling through the IL-21R, rather than interactions between IL-21 and a putative alternate receptor that may be expressed only on memory B cells and functions independently of

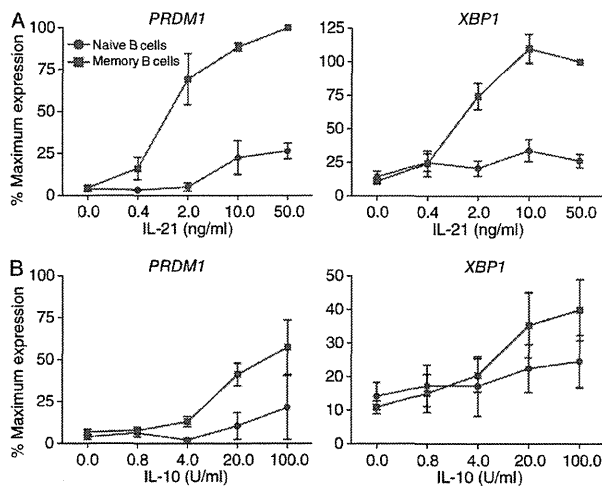


**Figure 6. Memory B cells exhibit greater sensitivity to the differentiation-inducing effects of STAT3-activating cytokines IL-21 and IL-10.** (A and B) Naive and memory B cells were sort-purified from normal donor spleens and then cultured with CD40L alone or with increasing concentrations of IL-21 (A) or IL-10 (B). After 4 d, expression of *PRDM1* and *XBP1* was determined by qPCR. The values are presented as the percentage of the maximum response, defined as the levels of expression induced in memory B cells by the highest dose of IL-21 tested (50 ng/ml). The data represent the mean  $\pm$  SEM of experiments using naive and memory B cells from three different normal donor spleens.

STAT3, we examined the B cell compartment in recently identified individuals with loss-of-function mutations in *IL21R* (Kotlarz et al., 2013). Phenotypic analysis of three individuals revealed a marked deficiency in memory B cells that was comparable with that observed for *STAT3*<sub>MUT</sub> patients (Fig. 7 A and Table 1). Furthermore, in contrast to healthy donors,  $\sim$ 95% of *IL-21R*<sub>MUT</sub> B cells were IgM<sup>+</sup>IgD<sup>+</sup>, revealing a deficiency in Ig isotype-switched cells (Fig. 7 B). We also quantified the proportion of memory B cells that expressed specific Ig isotypes and found that although  $\sim$ 50% of memory B cells from normal donors had lost expression of IgD and IgM,  $>$ 90% of *IL-21R*<sub>MUT</sub> memory B cells remained IgD<sup>+</sup> (Fig. 7 C and not depicted). Consistent with this,  $<$ 5% of *IL-21R*<sub>MUT</sub> memory B cells had undergone switching to express IgG or IgA, whereas the memory B cell pool of normal donors is comprised of  $\sim$ 25% IgG<sup>+</sup> and  $\sim$ 20% IgA<sup>+</sup> cells (Fig. 7 C). Thus, IL-21 signaling is indispensable for the generation of not only a normal pool of memory B cells but also the generation of isotype-switched effector B cells within the memory cell subset.

When naive B cells were isolated from normal donors and *IL-21R*<sub>MUT</sub> individuals and cultured in vitro, only B cells from normal donors responded to IL-21, as revealed by the generation of CD38<sup>hi</sup>CD27<sup>hi</sup> plasmablasts (Fig. 7 D), secretion of high levels of IgM, IgG, and IgA (Fig. 7 E), and down-regulation of *PAX5* while concomitantly acquiring *AICDA*, *PRDM1*, and *XBP1* expression (Fig. 7 F). All of these readouts of naive B cell differentiation were abolished by loss-of-function

mutations in *IL21R* (Fig. 7, D–F). Not surprisingly, CD40L-stimulated *IL-21R*<sub>MUT</sub> memory B cells also failed to respond to the stimulatory effects of IL-21 (Fig. 7 E). *IL-21R*<sub>MUT</sub> naive B cells, though, are intrinsically functional, as indicated by intact responses to IL-4 and IL-10 with respect to induction of *AICDA* (IL-4 and IL-10) and *XBP1* (IL-4) and reduction in *PAX5* (IL-10; Fig. 7 F). These findings demonstrate the specificity of the IL-21 used in our experiments and reveal that both naive and memory B cells absolutely require a functional *IL-21R* for their response to IL-21.

## DISCUSSION

Naive and memory B cells play distinct roles during humoral immune responses. Thus, naive B cells activated after primary encounter with foreign Ag initially produce Ag-specific IgM and eventually yield B cells that produce IgG or IgA. In contrast, memory cells respond much more efficiently upon subsequent exposure to such Ags, rapidly differentiating into Ab-secreting cells to produce substantially higher levels of protective Ig than naive cells (Ahmed and Gray, 1996; Rajewsky, 1996; Tangye and Tarlinton, 2009). This increased efficacy of memory B cell activation is one mechanism underlying long-term protective immunological memory.

B cell differentiation into plasmablasts is regulated by the integration of signals provided by Ag, T cell help (CD40L), and cytokines. Signal transduction pathways activated by these ligands converge to activate key transcriptional regulators, such as Blimp-1, that mediate the commitment of activated B cells to a PC fate (Nutt et al., 2011). Cytokines important for human B cell differentiation include IL-10 and IL-21, which induce isotype switching, PC generation, and Ab secretion from activated naive and memory B cells (Banchereau et al., 1994; Arpin et al., 1997; Pène et al., 2004; Ettinger et al., 2005; Bryant et al., 2007; Avery et al., 2008a). A common feature of these cytokines is their ability to activate similar signaling intermediates, such as STAT1 and STAT3. Remarkably, the effects of IL-10 or IL-21 on human naive B cells are abolished by heterozygous *STAT3* mutations, yet are unaffected by mutations in *STAT1* (Figs. 3–5; Avery et al., 2010). These defects likely explain defective Ab responses and reduced numbers of memory B cells in AD-HIES (Leung et al., 1988; Sheerin and Buckley, 1991; Avery et al., 2010) and, conversely, intact humoral responses in *STAT1*-deficient patients (Boisson-Dupuis et al., 2012). Interestingly, mutations in *IL21R* recapitulated the impaired Ab responses to vaccines (Kotlarz et al., 2013) and memory B cell deficit (Fig. 7) observed in AD-HIES, despite the ability of *IL-21R*-deficient B cells to respond to other growth and differentiation-inducing cytokines such as IL-4 or IL-10. In contrast, B cell responses in vivo appear intact in *IL-10/IL-10R*-deficient individuals (Kotlarz et al., 2012). Thus, STAT3, downstream of *IL-21R*, clearly plays a central role in establishing long-lived Ab-mediated immunity.

Our study revealed that *STAT3* mutations do not affect memory B cell function, as *STAT3*<sub>MUT</sub> memory cells underwent the molecular and cellular changes required for plasmablast

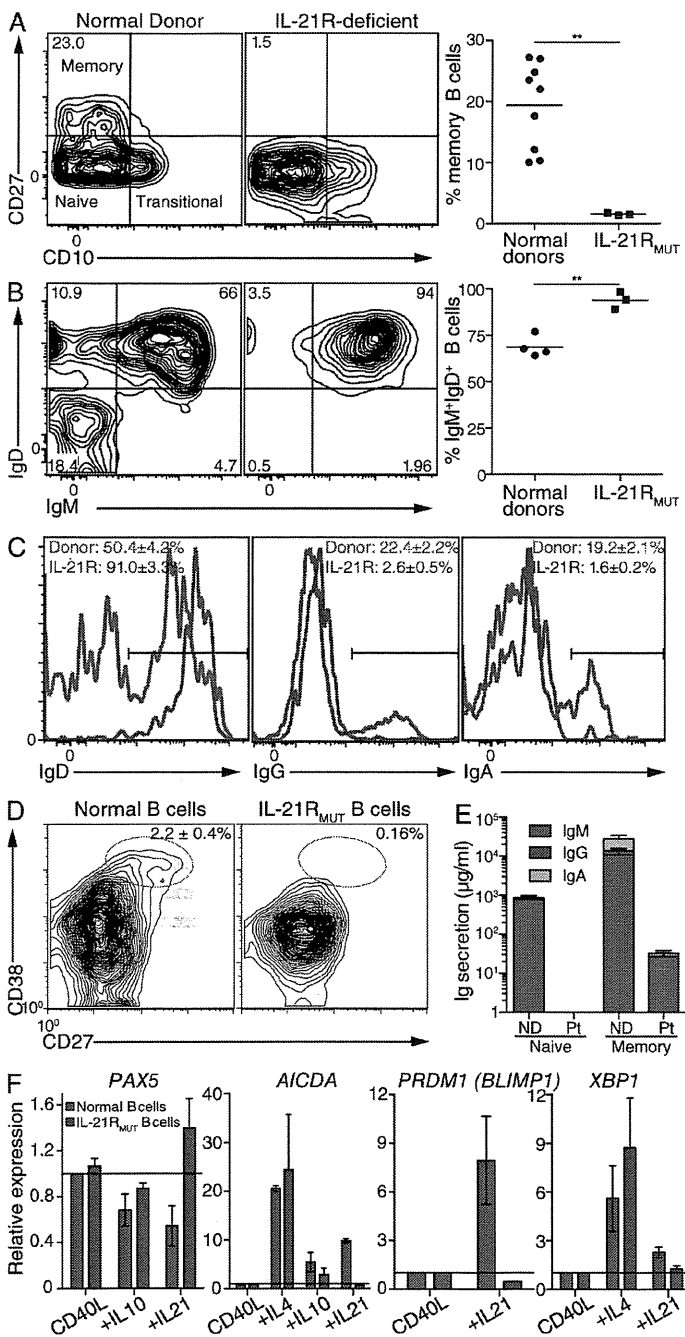


**Figure 7. Loss-of-function mutation in *IL21R* abolishes B cell responses to IL-21.** (A and B) PBMCs from age-matched normal donors and three patients with loss-of-function mutations in *IL21R* were labeled with mAb against CD20, CD10, CD27, IgM, IgD, IgG, and IgA. (A) Memory B cells were quantified based on the frequency of CD20<sup>+</sup> B cells that were CD10<sup>-</sup>CD27<sup>+</sup>. (B and C) The percentages of total B cells in normal donors or IL-21R-deficient patients that coexpressed IgM and IgD (B) and of memory (i.e., CD27<sup>+</sup>) B cells from normal donors and IL-21R<sub>MUT</sub> patients that expressed IgD, IgG, or IgA (C) were determined. \*\*, P < 0.01. Each symbol in A and B represents an individual normal donor or IL-21R<sub>MUT</sub> patient; the horizontal bars represent means. The values in C represent the mean percentage ± SEM of memory B cells from four normal donors or three IL-21R<sub>MUT</sub> patients that express IgD, IgG, or IgA. (D-F) Naive or memory B cells sort-purified from normal donors or IL-21R<sub>MUT</sub> patients were cultured with CD40L alone or CD40L/IL-21 (D and E) or CD40L/IL-4, CD40L/IL-10, or CD40L/IL-21 (F). After 5 d, the percentage of plasmablasts (i.e., CD38<sup>hi</sup>CD27<sup>hi</sup>) generated (D) and expression of *PAX5*, *AICDA*, *PRDM1*, and *XBP1* by cultured naive B cells (F) were determined by flow cytometry or qPCR. The values in D represent the mean (±SEM) percentage of naive B cells that acquired a plasmablast phenotype in response to CD40L/IL-21 in experiments using naive B cells from three different normal donors or one IL-21R<sub>MUT</sub> patient. In the absence of IL-21 <0.5% plasmablasts were detected in these cultures. (E) The levels of secreted IgM, IgG, and IgA by naive and memory B cells from normal donors (ND) or IL-21R<sub>MUT</sub> patients (Pt) in response to stimulation with CD40L/IL-21 were determined by ELISA after 10 d. The amounts of Ig secreted by IL21R<sub>MUT</sub> memory B cells in response to CD40L/IL-21 did not differ from those induced by CD40L alone (not depicted). These data are from one of three experiments using naive B cells from five different healthy controls or two unrelated IL-21R<sub>MUT</sub> patients. The values in F represent the mean ± SEM from experiments using two to five different healthy controls or of three experiments using cells from two unrelated IL-21R<sub>MUT</sub> patients. The horizontal black lines on the graphs in F indicate a value of 1.0, which corresponds to the relative level of expression of the indicated gene in CD40L-stimulated normal naive B cells.

differentiation in response to IL-10 or IL-21. Importantly, although memory cells are numerically deficient in AD-HIES patients, they produced normal levels of Ag-specific IgG in vitro on a per cell basis, inferring that STAT3<sub>MUT</sub> memory B cells would be functional in vivo. This explains the variability in impairment in humoral immunity in AD-HIES patients (Sheerin and Buckley, 1991; Avery et al., 2010). There are several explanations for the normal response of STAT3<sub>MUT</sub>

memory B cells to STAT3 cytokines. First, these cytokines may activate signaling pathways in memory B cells distinct from naive cells, thereby allowing memory cells to respond independently of STAT3, unlike naive B cells. This is unlikely as we detected comparable activation of STATs, yet little activation of Erk and Akt in IL-21-stimulated naive and memory B cells. Second, STAT3 may be differentially expressed by naive and memory B cells; however, this was also

found to not be the case. Third, because STAT1<sub>MUT</sub> B cells secreted less Ig in vitro over time, STAT1 may contribute to the function of activated memory B cells. Even if correct, the reduction in Ig secretion by STAT1<sub>MUT</sub> memory B cells is probably not physiologically significant as these patients have intact humoral immunity (Boisson-Dupuis et al., 2012). This may reflect the intact early differentiation of STAT1<sub>MUT</sub> naive and memory B cells in response to IL-10 and IL-21 in vitro, the generation of normal numbers of memory B cells in vivo, and the ability of STAT1<sub>MUT</sub> memory B cells to produce sufficient quantities of specific Abs after reexposure to immunizing Ags or infectious pathogens. These findings suggest that STAT1 plays only a minor, if any, role in inducing and maintaining humoral immunity. A final possibility is that memory B cells require less activated STAT3 to respond to specific cytokines than do naive B cells. Thus, the residual amounts of functional STAT3 in STAT3<sub>MUT</sub> B cells are sufficient to mediate plasmablast differentiation induced by IL-10 and IL-21 in memory, but not naive, B cells. This is supported by our finding that IL-10 and IL-21 induced expression of the key PC transcription factors Blimp-1 and XBP-1 in memory B cells at concentrations that had no effect on gene expression in corresponding naive B cells (Fig. 6). This, therefore, is our favored model, which is also consistent with memory B cells having a lower threshold for activation than naive B cells (Yefenof et al., 1986; Poudrier and Owens, 1994), which underlies their rapid response on subsequent encounters with specific Ag (Ahmed and Gray, 1996; Rajewsky, 1996; Tangye and Tarlinton, 2009; Goodnow et al., 2010).

These findings also provide important insights into the hierarchy by which cytokines operate to induce B cell differentiation. Thus, although IL-21R-deficient naive B cells could respond to IL-4 and IL-10 in vitro to induce key events required for Ig isotype switching (*AICDA* expression) and PC generation (*PRDM1* and *XBP1*), responses to these and other cytokines such as BAFF and APRIL (Banchereau et al., 1994; Litinskiy et al., 2002; Avery et al., 2003; Craxton et al., 2003) are insufficient in vivo to compensate for a complete absence of IL-21/IL-21R signaling. This is indicated by B cells in IL-21R-deficient individuals expressing only IgM and IgD, with essentially no isotype-switched cells being detected (Fig. 7). Thus, despite IL-4 and IL-10 inducing *AICDA* expression in IL-21R-deficient B cells, a primary signal via the IL-21R appears to be the critical and rate-limiting step for B cells to undergo isotype switching, after which cytokines such as IL-4, IL-10, BAFF, and APRIL can cooperate to enhance IL-21-induced switching and B cell differentiation (Litinskiy et al., 2002; Avery et al., 2003, 2008a; Craxton et al., 2003). This is reminiscent of the immunological phenotype of X-linked or JAK3-deficient SCID patients who have undergone stem cell transplant but retain autologous (i.e., *IL2RG* or *JAK3* mutant) B cells, inasmuch that these patients have significant reductions in memory B cells, isotype-switched B cells, and serum IgM and lack serum IgG and IgA (Recher et al., 2011), thereby highlighting the

requirement for intact signaling through  $\gamma$ c/JAK3 downstream of IL-4R and IL-21R for B cell differentiation and effector function. Interestingly though, populations of IgG<sup>+</sup> and IgA<sup>+</sup> cells were detectable within the memory B cell subset of STAT3-deficient individuals, despite the reduction in total memory B cells in these patients. Because IL-21 could induce CD40L-activated STAT3<sub>MUT</sub> naive B cells to express *AICDA*, but not *PRDM1*, it is likely that the level of STAT3 required to mediate class switching in naive B cells is significantly less than that required for plasmablast formation. Thus, although IL-21R is indispensable for class switching in vivo, the residual amount of functional STAT3 in STAT3<sub>MUT</sub> naive B cells is sufficient to mediate IL-21-induced class switching in vivo. These findings demonstrate that within the same cell type (i.e., naive B cells) the thresholds of activation of STAT3 required for different biological processes (i.e., class switching versus plasmablast generation) are distinct, thereby providing a rational explanation for (a) intact class switch recombination but defective plasmablast formation by STAT3-deficient naive B cells to IL-21 and (b) phenotypic differences between memory B cells in patients with mutations in *STAT3* or *IL21R*.

As a key attribute of memory B cells is their ability to respond more rapidly than naive B cells, a question that arises is why STAT3<sub>MUT</sub> memory B cells do not increase in frequency over time to improve humoral immunity in AD-HIES. Because STAT3<sub>MUT</sub> memory B cells exhibit normal responses to IL-21 in vitro, this would suggest that availability of, or access to, stimulatory cytokines in vivo is limiting. We have reported that the proportions (Ma et al., 2012; Mazerolles et al., 2013) and absolute numbers ( $101 \pm 7$  cells/ml in normal donors vs.  $51.6 \pm 10$  cells/ml peripheral blood in STAT3 deficiency) of circulating CD4<sup>+</sup>CXCR5<sup>+</sup> T cells, which like Tfh cells present in secondary lymphoid tissues are enriched for IL-21-producing cells (Chevalier et al., 2011), are reduced in AD-HIES patients. Furthermore, STAT3<sub>MUT</sub> CD4<sup>+</sup> T cells are impaired in their ability to generate Tfh-like cells in vitro, thereby compromising IL-21-mediated help for B cell differentiation (Ma et al., 2012). These observations are consistent with a scenario whereby STAT3<sub>MUT</sub> memory B cells, despite their intact ability to respond to IL-21, are constrained in doing so in vivo because of diminished production of IL-21 by STAT3-deficient CD4<sup>+</sup> T cells.

The deficit in memory B cells observed in STAT3<sub>MUT</sub> patients is comparable with that in other immune-deficient individuals, such as patients with mutations in *SH2D1A* (XLP; Ma et al., 2005, 2006), *CD40LG* (hyper-IgM syndrome; Notarangelo et al., 2006) or *ICOS* (common variable immunodeficiency; Warnatz et al., 2006), or transplanted X-linked/JAK3-deficient SCID patients who retain autologous B cells (Recher et al., 2011). Although all of these latter conditions are characterized by reductions in serum Ig levels (Ma et al., 2005; Notarangelo et al., 2006; Warnatz et al., 2006; Recher et al., 2011), serum levels of IgM, IgG, and IgA are normal in STAT3-deficient patients despite a generalized impairment in the ability to elicit sustained Ag-specific Ab

responses (Leung et al., 1988; Sheerin and Buckley, 1991; Avery et al., 2010). Our results provide a potential explanation for the apparent discrepancy between reduced memory B cells but normal serum Ig levels in STAT3 deficiency, inasmuch that the residual memory B cells can respond to B cell differentiating cytokines and thus contribute to the pool of serum Ig. The corollary of this is that the small population of memory B cells in XLP, hyper-IgM syndrome, ICOS deficiency, and posttransplant SCID are unable to access appropriate CD4<sup>+</sup> T cell-derived signals (i.e., SAP-dependent interactions; CD40L; ICOS; IL-2/IL-4/IL-21) and thus are limited in their ability to contribute to humoral immunity. An extension of our findings is that because we could detect functional Ag-specific STAT-3<sub>MUT</sub> memory B cells, directed targeting of these cells with IL-21-mediated signals may improve humoral immunity in AD-HIES patients.

## MATERIALS AND METHODS

**Human blood and tissue samples.** Buffy coats and spleens from healthy donors were provided by the Australian Red Cross Blood Service. Peripheral blood was also collected from patients with loss-of-function mutations in *STAT1* (STAT1<sub>MUT</sub>; Dupuis et al., 2001; Chaggier et al., 2006, 2009; Sampaio et al., 2012; Hirata et al., 2013; Ives et al., 2013), *STAT3* (STAT-3<sub>MUT</sub>; Ma et al., 2008, 2012; Avery et al., 2010) or *IL21R* (IL-21R<sub>MUT</sub>; Kotlarz et al., 2013; Ives et al., 2013; Table S1). Approval for this study was obtained from the human research ethics committees of the St. Vincent's Hospital and Sydney South West Area Health Service (Australia), the Rockefeller University Institutional Review Board (New York), and the National Institute of Allergy and Infectious Diseases Intramural Institutional Review Board (Bethesda, MD).

**Lymphocyte phenotyping and isolation.** PBMCs were incubated with mAb to CD20 and CD27 and an isotype control or mAb specific for CD23, CD24, CD80, CD86, CD95, TACI, IgM, IgD, IgG, IgG1, IgG2, IgG3, IgG4, and IgA, and expression of these molecules on CD20<sup>+</sup>CD27<sup>-</sup> (naive) and CD20<sup>+</sup>CD27<sup>+</sup> (memory) B cells was determined by flow cytometry (Ma et al., 2006). Naive and memory B cells were purified by labeling either PBMCs or total B cells with mAb against CD10, CD20, and CD27 and sorting CD10<sup>-</sup>CD20<sup>+</sup>CD27<sup>-</sup> (naive) and CD10<sup>-</sup>CD20<sup>+</sup>CD27<sup>+</sup> (memory) cells (FACSaria; BD; (Avery et al., 2008b, 2010). Spleenic B cells were labeled with mAbs against CD20, CD27, IgG, and IgA, and subsets of either naive (CD20<sup>+</sup>CD27<sup>-</sup>) and total memory B cells (CD20<sup>+</sup>CD27<sup>+</sup>) or IgM memory (CD20<sup>+</sup>CD27<sup>-</sup>IgG-IgA<sup>-</sup>) and isotype-switched (CD20<sup>+</sup>CD27<sup>-</sup>IgG<sup>+</sup>IgA<sup>+</sup>) memory B cells were collected (FACSaria; Tangye et al., 2003a; Bryant et al., 2007; Good et al., 2009). The purity of the recovered populations was typically >98%. To enumerate circulating Tfh-like cells, PBMCs were labeled with mAbs against CD3, CD4, and CXCR5, and the absolute number of CD4<sup>+</sup>CXCR5<sup>+</sup> T cells was then determined.

**In vitro activation of naive and memory B cells.** Naive and memory B cells isolated from normal donors or STAT3<sub>MUT</sub>, STAT1<sub>MUT</sub>, or IL-21R<sub>MUT</sub> patients were cultured (~5–10 × 10<sup>5</sup>/200 μl/well for proliferation, Ig secretion, and qPCR and ~4 × 10<sup>4</sup>/400 μl/well for phenotyping; BD) with CD40L alone or together with 100 U/ml IL-4, 100 U/ml IL-10, 50 ng/ml IL-21 (PeproTech), or 1 μg/ml CpG 2006 (Sigma-Aldrich). Expression of *STAT3*, *PAX5*, *PRDM1*, *XBP1*, *IRF4*, and *AICDA* was determined after 5 d by real-time PCR and standardized to *GAPDH* (Avery et al., 2010). Expression of Ig  $\epsilon$  germline transcripts were determined by PCR as described previously (Avery et al., 2008b). Differentiation of B cells to plasmablasts was assessed by determining the frequency of cells acquiring a CD-38<sup>hi</sup>CD27<sup>hi</sup> phenotype during in vitro culture (Avery et al., 2005). B cell proliferation was determined by assessing the incorporation of [<sup>3</sup>H]thymidine (1 μCi/ml per well; ICN Biomedicals) during the final 18 h of a 5-d culture

(Good et al., 2006). Ig secretion was determined by ELISA after 4–12 d of culture (Bryant et al., 2007). Relative levels of antitetanus IgG in culture supernatants were determined by ELISA using plates precoated with tetanus toxoid (Sigma-Aldrich) and then detecting bound IgG (Avery et al., 2010).

**Analysis of intracellular signaling.** Naive and memory splenic B cells were cultured with F(ab')<sub>2</sub> fragments of goat anti-human Ig (Jackson Immuno-Research Laboratories, Inc.) for ~18 h, washed, and then recultured with media alone, 100 ng/ml IL-21, or F(ab')<sub>2</sub> anti-Ig for 15–30 min. Cells were then fixed, permeabilized, labeled with anti-phospho-STAT1, STAT3, STAT4, STAT5, and STAT6 mAb (Avery et al., 2008b, 2010) and analyzed by flow cytometry. Alternatively, cells were lysed and Western blotting was performed using rabbit polyclonal anti-STAT3 (C-20), anti-ERK2 (C-14), and anti-14.3.3 (K-19; Santa Cruz Biotechnology, Inc.); and anti-STAT3 pY705 (3E2), anti-AKT pS473 (587F11), and anti-ERK1/2 pT202/Y204 (Cell Signaling Technology).

**Statistical analysis.** Significant differences between datasets were determined using either the unpaired Student's *t* test when comparing two variables or ANOVA for more than two variables (Prism; GraphPad Software).

**Online supplemental material.** Table S1 provides details of the patients analyzed in this study. Online supplemental material is available at <http://www.jem.org/cgi/content/full/jem.20130323/DC1>.

We thank the Garvan Flow Cytometry facility for cell sorting, Rob Brink, Tri Phan, and Tony Basten for critical review of this manuscript, members of the James laboratory (Garvan Institute) for advice on Western blotting, and the patients and their families for participating in this project. We also acknowledge the late Dr. Klaus Madgorf for his contributions to our research.

This work was funded by project and program grants from the National Health and Medical Research Council (NHMRC) of Australia (to E.K. Deenick, C.S. Ma, D.A. Fulcher, M.C. Cook, and S.G. Tangye) and the Rockefeller University Center for 541 Clinical and Translational science (5UL1R024143 to J.L. Casanova). C.S. Ma is a recipient of a Career Development Fellowship, L.J. Berglund is a recipient of a Medical Postgraduate Scholarship, and S.G. Tangye is a recipient of a Principal Research Fellowship from the NHMRC of Australia. L. Moens is the recipient of a Postdoctoral Fellowship from the Research Foundation-Flanders (FWO), Belgium.

The authors declare no competing financial interests.

Submitted: 12 February 2013

Accepted: 22 October 2013

## REFERENCES

- Ahmed, R., and D. Gray. 1996. Immunological memory and protective immunity: understanding their relation. *Science*. 272:54–60. <http://dx.doi.org/10.1126/science.272.5258.54>
- Arpin, C., J. Banachereau, and Y.J. Liu. 1997. Memory B cells are biased towards terminal differentiation: a strategy that may prevent repertoire freezing. *J. Exp. Med.* 186:931–940. <http://dx.doi.org/10.1084/jem.186.6.931>
- Asao, H., C. Okuyama, S. Kumaki, N. Ishii, S. Tsuchiya, D. Foster, and K. Sugamura. 2001. Cutting edge: the common gamma-chain is an indispensable subunit of the IL-21 receptor complex. *J. Immunol.* 167:1–5.
- Avery, D.T., S.L. Kalled, J.I. Ellyard, C. Ambrose, S.A. Bixler, M. Thien, R. Brink, F. Mackay, P.D. Hodgkin, and S.G. Tangye. 2003. BAFF selectively enhances the survival of plasmablasts generated from human memory B cells. *J. Clin. Invest.* 112:286–297.
- Avery, D.T., J.I. Ellyard, F. Mackay, L.M. Corcoran, P.D. Hodgkin, and S.G. Tangye. 2005. Increased expression of CD27 on activated human memory B cells correlates with their commitment to the plasma cell lineage. *J. Immunol.* 174:4034–4042.
- Avery, D.T., V.L. Bryant, C.S. Ma, R. de Waal Malefyt, and S.G. Tangye. 2008a. IL-21-induced isotype switching to IgG and IgA by human naive B cells is differentially regulated by IL-4. *J. Immunol.* 181:1767–1779.
- Avery, D.T., C.S. Ma, V.L. Bryant, B. Santner-Nanan, R. Nanan, M. Wong, D.A. Fulcher, M.C. Cook, and S.G. Tangye. 2008b. STAT3 is required